Response to Reviewer #1

We are thankful to prof. Cassiani for his valuable comments and suggestions, which have certainly improved the manuscript. The response to the individual comments is given below. The original review is quoted in *italics*, whereas our response is given in **bold**.

(1) *I have found the paper interesting and potentially worth publication. However I find it somewhat surprising that the authors seem to believe that TDR is a better method than EMI to measure electrical conductivity. This seems to be an assumption made a priori, and not supported either by the scientific literature nor by any evidence in the paper. EMI is designed specifically to measure electrical conductivity, while TDR is designed with the measurement of dielectric properties in mind. Using TDR also to measure electrical conductivity can be done, similarly to using attenuation in GPR measurements to do the same. However it is not a recommended approach. My suggestion to the author is to reverse the line of reasoning, believe more in EMI (with some caveats especially concerning the depth of investigation) and rather question TDR as a method for sigma measurement. In a nutshell, give more credibility to geophysics and question some belief in soil science. To this end, I also suggest that an eye is given to ERT as a technique that can provide ground truth much more reliable that TRD for electrical conductivity (see e.g. Cassiani et al., 2012 and Ursino et al., 2014, but many other papers deal with the EMI-ERT obvious relationship). I am also very surprised that moisture content estimates from TDR are not considered at all in the paper – yet the data must be available. I suggest the authors present also those (much more solid, I presume) data. I encourage the authors to revise the paper along these lines and resubmit this potentially interesting dataset.*

Concerning the effectiveness and accuracy of electrical conductivity measurements via TDR, consistently with our previous reply to the Reviewer, we largely extended the discussion in the revised version of the manuscript and added several references supporting the rationale behind our approach.
We believe that, in the new manuscript, the limits of validity of the presented workflow for the calibration of the EMI inversion results by using TDR measurements are now better defined and the associated assumptions are more clearly explained.

(2) *Line 26: "contributing to enhance the spatial resolution of the EMI reconstruction". I am not sure one can claim that the use of a stabilizer (how much needed would also require a specific discussion) truly enhances spatial resolution of a geophysical method. In my opinion this statement is wrong. I suggest a reformulation here.*

With that statement, we simply mean that the appropriate regularization can increase the capability to distinguish blocky anomalies. In fact, "standard" (smoothing) stabilizers, when blindly applied to targets with sharp boundaries, generally result in a significant reduction of the resolution capabilities as they tend to smear the anomalies out. The

contrary is true for sharp inversion algorithms (clearly only when they are applied to soils characterized by abrupt changes in the property under investigation).

However, we see the point of the Reviewer and, in the new version of the paper, we modified all the parts dealing with the enhanced resolution capabilities of the sharp inversion to better explain what we actually mean and to limit the risks of misunderstandings.

(3) *Line 35: "after filtering the TDR data" Even though this is the abstract, the statement is far too generic. Details about the filtering approach shall be briefly given here.*

Accordingly to the Reviewer's suggestion, in the new version of the abstract, we added more details about the TDR data filtering. Moreover, in the rest of the article, we significantly extended the part concerning the strategy to design the optimal filtering and, on the other hand, removed the long portion devoted to the description of the Fourier Transform.

(4) *Line 125: "Then we assess the quality of these reconstructions by using TDR data as ground-truth." This is a very brave statement. I do not see TDR as any more reliable to measure sigma than EMI, indeed quite the opposite. Line 132:"Accordingly, the paper provides a methodology to calibrate EMI results by TDR readings." This should not (cannot) be the focus of this paper. If the authors believe this is a viable strategy, I totally disagree.*

On this respect, kindly, see our previous reply to comment # 1.

(5) *Line 291 and following. Spending time describing Fourier transformation is probably useless. Rather, I would concetrate on describing in detail what type of filtering is applied. "Fourier filtering" is unclear. I presume it is a spatial filtering made to enhance the long wavelengths? Please be more specific and try and link the approach to established (there are far too many) filtering techniques.*

We definitely see the Reviewer's point. As already mentioned in our reply to comment # 3, in the new version, we removed the Fourier Transform description and focused on the discussion of the utilzed filter.

(6) *Line 573: "Ferre" is actually "Ferré".*

This typo is now corrected.

(7) *Line 727 Figure 2. "Examples of sharp and smooth inversions applied to the same dataset 100-6dS. The results are shown together with their corresponding data misfit". I see only one curve of data misfit. Does it refer to both sharp and smooth inversion? Also, I find it a bit difficult to justify in the images how some dark blue areas in the smooth inversion indeed correspond to slightly less dark blue areas in the sharp inversion. I am also a bit skeptical of the fact that using an EM38 one can image with confidence to a depth as large as 3 m!.*

Actually, the original Fig. 2 was already showing both (sharp and smooth) data misfits for the 100-6dS case. However, in the new version, also following the suggestions of the Reviewer #2, we decided to: (i) improve the clarity of the data misfit plot of the original Fig. 2; (ii) include a similar figure for the 50-6dS case (the new Fig. 3); (iii) add a figure, for each of the 100-6dS and 50-6dS cases, showing the observed and calculated data corresponding to the sharp and smooth reconstructions. These additional figures further demonstrate the ill-posedness of the inversion problem (in particular in presence of a very limited number of observations with relatively high levels of noise). In fact, it is clear from the new Fig.s 2-5 that, despite the data fittings are very similar, the sharp and smooth inversions provide significantly different results in all the considered cases.

Concerning the section depth, we are not necessarily claiming that the EM38 is actually investigating down to 3 m. After all, we use only the first 0.6 m along the paper. To some extent, we decided to "over-parametrize" the model (for example, in terms of number and density of the layers) to prevent any possible side-effects and to let the regularization be uniquely controlled by the stabilizer. In the new manuscript, we have added a few lines about these aspects.

(8) *Line 735, Figure 3:here too some details about the filter applied to the TDR data shall be given. It is not acceptable that in a caption only the term "filtered" is applied. One can use any type of filter! The same applies to Figures 4 and 5.*

Please, see our reply to the comment # 3.

(9) *Figure 6: the difference between TDR and EMI measured sigma is quite large indeed. Overall I am not sure that TDR is the best method to measure sigma. Indeed it is not. TDR is the chief approach to measure dielectric properties.*

The difference in the original Fig. 6 is not surprising as, for example, it is well-known that EMI measurements require frequent calibrations (just as an example, see Lavoué et al., 2010, Electromagnetic induction calibration using apparent electrical conductivity modelling based on electrical resistivity tomography. Near Surface Geophysics 8(6),

553-561). And this is why we developed a calibration strategy for the EMI results based on the TDR measurements. Regarding the appropriateness of using TDR as reliable methodology to retrieve the true soil conductivity, please, see our reply to comment # 1.

(10) *Figure 8: the difference between the two images is striking. I am not sure how the authors are so confident that the correction applied to obtain the revised EMI image is correct.*

In the revised version of the manuscript, we completely modify the original Fig. 8 (corresponding now to Fig. 10). The new Fig. 10 shows the calibration results for all transects and demonstrates that the proposed strategy preserves the spatial variability of the EMI reconstruction but with conductivity ranges compatible with the TDR measurements (here assumed to be reliable estimation of the true soil conductivity).

Response to Reviewer #2

We thank Reviewer #2 for his/her valuable comments and suggestions, which have certainly improved the manuscript. The response to the individual comments is given below. The original review is quoted in *italics*, whereas our response is given in **bold**.

(1) *TDR conductivity measurements show larger conductivity close to the surface as it should be expected since it is closer to the source of conductive material (added saline water). For this aspect, it is acceptable to consider TDR conductivity measurements as providing more reliable information, which could serve to calibrate "less reliable conductivities" obtained with EMI measurements (or their inversion). I therefore agree with the overall approach. I find the paper clear and well-written. I have nevertheless few questions at the EMI inversion stage which, I think, should be explored, or at least discussed before acceptance. I also think that Authors should show the final results for the other transects in order to see if the calibration performs well for the different irrigation experiments. This being said, this manuscript is interesting as it addresses the problem of relating ground truth and EMI output with a pragmatic approach.*

We agree with the Reviewer's remarks. Accordingly, in the revised version of the manuscript, we further elaborated on the role and importance of the assumptions made during the inversion stage and also shown the results from all the other transects.

(2) *Non-uniqueness of the conductivity model resulting from the inversion:*
One particular choice of the present study (compared to other cited studies) is to calibrate the conductivity after inversion instead of EMI apparent conductivity data (Eca). However, the argument of non-uniqueness of the inverse problem, which is actually used by the authors in the introduction to question a calibration with ERT method, could be used here in the same way to question the presented method.

In the new version of the paper, we stressed this aspect and made our point clearer. So, we further elaborated on the fact that all the limitations/assumptions connected with the ill-posedness of the EMI inversion are inevitably inherited by our approach.

We also added a brief discussion on a possible alternative strategy to use the TDR measurements to calibrate directly the EMI-EC$_a$ data (data-space calibration). This second option would not need any statistical analysis of the data since the physics of the EMI forward modelling would effectively perform the rescaling. However, eventually, also in this case, when it is time to translate the (now calibrated) EMI-EC$_a$ into the corresponding conductivities $\sigma_{b,EMI}$, it will be necessary to go through the inversion process (with all its associated assumptions).

As it is discussed in the new manuscript, we opted for the model-space calibration for pragmatic reasons connected with the possible difficulties to decuple the forward modelling parts in the, usually available, EMI inversion codes.

(3) *This said, are you sure that the selected solution obtained using sharp regularization is the best solution to be compared with TDR? Actually, some of the smooth models (e.g. sounding numbers 5 , 13 17 in Figure 2) show better vertical concordance with what should be expected and with the best misfit. Anyway, Figure 2 clearly highlights the non-uniqueness of the problem, because it is possible to obtain very different models at similar misfits. Why, for example, not putting some effort to stabilize the regularization of the smooth inversion in order to have sounding N5-like results all along the transect? I do see that, because of fixed interfaces and a very little number of layers, your parameterization does not allow enough model space flexibility to have stable smooth results along the transect. But there are many ways to fix such issues (like, for example, among others, increasing the number of layers or applying some lateral constraints). I would also like to point out that the smooth misfits are slightly higher than for the sharp method (of 1-2 %, except for the few soundings mentioned above. This feature supports my previous comments), which is not in favor of the smooth regularization in a context of fair comparison. For all this, I would not qualify the smooth inversions presented here as a "standard" approach as it is not used with an optimal way (you use few layers with fixed interfaces). For Figure 2, I really recommend to plot the profiles of collected EMI data together with modeled (after inversion) data to see exactly how well all the channels were fitted. This would allow to properly evaluate and discuss the two methods of inversions. This is also important for a second aspect : in a cultivated area, I would expect some lateral anisotropy of the conductivity of the soil layer due the preferential orientation of the lines of the agricultural work. If this is true, inverting HCP and VCP together would not be an optimal choice as such geometries induce eddy current with different preferential directions. Did you try to consider HCP only, and/or VCP only? Maybe there would be a better qualitative and quantitative consistency between TDR and EMI inversion results?*

The Reviewer correctly highlighted that we used fix interfaces in our model parameterization. However, we have used a discretization with 100 layers down to 8 m depth to be sure: (i) to control the inversion results by acting only on the regularization parameters and (ii) to remove the regularization effects possibly originated by the discretization choices (e.g., the number of layers, interfaces locations). In this way, we have been able to use an automatic strategy for the selection of the regularization parameters. For these reasons, we believe that our smooth result can be defined "standard". We added to the new manuscripts a few lines about this to better explain our point.

Regarding the use of lateral constraints, it can definitely be a viable solution, but we showed that a satisfactory lateral consistency can be achieved by using an already existing 1D code (slightly modified to accommodate a sharp regularization) instead of implementing a (clearly more troublesome to code) pseudo-2D (e.g., laterally constrained) version of it.

Moreover, from our point of view, the fact that the data misfits are largely overlapping, confirms that the two inversion results are actually comparable. And, if the sharp inversion fits better the data, the simplest explanation

might be that the assumption of sharp interfaces is in a better agreement with the reality and that the (blocky) true model is difficult to be correctly retrieved when smooth constraints are applied.

These arguments are confirmed by the results for all transects. On this respect, in the revised paper, we included an additional new figure (Fig. 4) showing a consistent behaviour also for the 50-6dS case.

We totally agree with the reviewer that the best way to assess the quality of the data fitting is to plot the collected data against the calculated ones. So, in the revised manuscript, we added two new figures on this respect (Fig.s 3 and 5).

(4) *To sum up, I would have interpreted the results shown in Figure 2 in a different manner. After acceptation of the non-uniqueness of the EMI data inversion, I would have tried to find the right parameterization and regularization to get sounding N5-like results along the transect before starting the comparison with TDR. As a consequence, I believe that the calibration procedure presented in this study also corrects error due to the non-uniqueness inherent to the considered inverse problem (in addition to the spatial fractality problem already discussed in the text). And in the eventual case of lateral anisotropy, it maybe also correct for less realistic EMI results resulting from joint HCP and VCP inversion. However this two features means that the overall calibration procedure could be dependent on the initial method of inversion. In my opinion, this aspect should be explored in this study, or at least discussed in the text.*

Kindly see our previous replies to comments # 1-3.

(5) *Application of the method to the four transects:*

I think you should show the resulting sections (like Figure 8) for all the transects in order to check the consistency of the calibration procedure over larger areas (and implicitly for broader geological/irrigation settings) as it is claimed in the conclusion.

We definitely see the rationale behind Reviewer's remark and, in the new version, we showed the results from all transects. They confirm the robustness and reliability of the proposed calibration approach.

(6) *Some minor comments:*

In the discussion about magnetic permeability (p7 line 239-241), you cite a nonpublished paper (Deidda et al, submitted). Here, it is necessary to also cite already published papers on this topic. There are a couple of recent studies dealing with the inversion of in-phase data for retrieving the magnetic permeability for the case of small EMI sensors.

Following the Reviewer's suggestion, we included the references to additional relevant studies.

(7) *Figure 8 shows spectacularly that the TDR conductivity of the first layer is largely underestimated by the EMI sharp inversion results. Are we sure that this first layer is well constrained by the considered EMI vertical soundings? Maybe it would be good to show and analyze the a priori covariance on model parameter associated to the selected 4-heights/2-geometries data set.*

The original Fig. 8 (now Fig. 10) has been largely revised, and, now, it is not subdivided into three layers anymore. The new final results (Fig. 10d-g) show significant improvements as they effectively merge the information contents of the two original datasets. In fact, at the same time, they preserve the spatial variability (over relatively large areas) of the EMI model together with the reliable conductivity ranges supplied by the TDR measurements.

(8) *Summary of my recommendations:*

Plot the measured data versus the modeled data in Figure 2. Explore or discuss the dependence of the overall procedure on the method of inversion. Show the final results for the four transects to confirm the robustness of the method on different irrigation contexts.

Once again, we thank the Reviewer for his/her useful and pertinent comments and suggestions. As mentioned above, in the new manuscript, we showed the measured vs calculated data, made our point clearer regarding the dependence on the adopted inversion strategy, presented the results from the other transects.

CALIBRATING ELECTROMAGNETIC INDUCTION CONDUCTIVITIES WITH TIME-DOMAIN REFLECTOMETRY MEASUREMENTS

Dragonetti[1] Giovanna, Alessandro Comegna[2], Ali Ajeel[2], Gian Piero Deidda[3], Nicola Lamaddalena[1], Giuseppe Rodriguez[4], Giulio Vignoli[3,5], Antonio Coppola[2]*

(1) Mediterranean Agronomic Institute (MAIB) - Land & Water Department, Valenzano (Bari), Italy

(2) University of Basilicata, School of Agricultural, Forestry and Environmental Sciences - Hydraulics and Hydrology Division, Potenza, Italy. e-mail: antonio.coppola@unibas.it

(3) Dipartimento di Ingegneria Civile, Ambientale e Architettura, Università di Cagliari, Cagliari, Italy

(4) Dipartimento di Matematica e Informatica, Università di Cagliari, Cagliari, Italy

(5) Groundwater and Quaternary Geology Mapping Department, Geological Survey of Denmark and Greenland, Aarhus, Denmark

Abstract

This paper deals with the issue of monitoring the ~~horizontal and vertical~~spatial distribution of bulk electrical conductivity~~,~~ σ_b, in the soil root zone by using Electromagnetic Induction (EMI) sensors under different water and salinity conditions. ~~In order t~~To deduce the actual distribution of depth-specific σ_b from EMI ~~depth-weighted~~ apparent electrical conductivity (EC_a) measurements, we inverted the ~~signal~~ data by using a regularized 1D inversion procedure designed to manage nonlinear multiple EMI-depth responses. The inversion technique is based on the coupling of the damped Gauss-Newton method with truncated generalized singular value decomposition (TGSVD). The ill-posedness of the EMI data inversion is addressed by using a sharp stabilizer term in the objective function. This specific stabilizer promotes the reconstruction of blocky targets, thereby contributing to enhance the spatial resolution of the EMI ~~reconstruction~~results in presence of sharp boundaries (otherwise smeared out after the application of more standard, Occam-like regularization strategies searching for smooth solutions). Time-Domain Reflectometry (TDR) data are used as ground-truth data for calibration of the inversion results. An experimental field was divided into four transects 30 m long and 2.8 m wide, cultivated with green bean and irrigated with water at two different salinity levels and using two different irrigation volumes. Clearly, this~~,~~ ~~to~~ induced different salinity and water contents within the soil profiles. For each transect, 26 regularly spaced monitoring ~~sites~~ soundings (1 m apart) were selected for ~~soil~~ the collection ~~measurements using~~of, respectively: (i) ~~a~~ Geonics EM-38 and (ii)~~a~~ Tektronix Reflectometer data. Despite the original discrepancies in the EMI and TDR data, we found a significant~~ly~~ ~~high~~ correlation of the means and standard deviations of the two data series,~~;~~ ~~especially~~ in particular, after a low-pass spatial filtering of the TDR data. Based on these findings, the paper introduces a novel methodology to calibrate EMI-based electrical ~~conductivity~~ conductivities via TDR direct measurements. This calibration strategy consists in a linear mapping of the original inversion results into a new conductivity spatial distribution with the coefficients of the transformation uniquely based on the ~~by simply using the~~ statistics of the two original measurement datasets (EMI and TDR conductivities) ~~series~~.

Introduction

Soil water content and salinity vary in space both vertically and horizontally. Their distribution depends on management practices and on the complex nonlinear processes of soil water flow and solute transport, resulting in variable storages of solutes and water (Coppola et al. 2015).

Monitoring the actual distribution of water and salts in the soil profile explored by roots is crucial ~~to~~ for managing irrigation with saline water, while still maintaining an acceptable crop yield. For ~~monitoring~~ water and salts monitoring over large areas, there are now non-invasive techniques based on electromagnetic sensors which allow the bulk electrical conductivity of soils~~,~~ σ_b~~,~~ to be determined (Sheets and Hendrickx 1995, Corwin and Lesch 2005, Robinson et al. 2012, Doolittle and Brevik 2014, ~~von Hebel et al. 2014~~Von Hebel et al. 2014), among many others).

σ_b depends on: (i) ~~on~~ soil water content~~,~~ θ;~~,~~ (ii) electrical conductivity of the soil solution (salinity)~~,~~ σ_w;~~,~~ (iii) tortuosity of the soil-pore system~~,~~ τ;~~,~~ and (iv) other factors related to the solid phase such as bulk density, clay content and mineralogy.

Electromagnetic induction (EMI) sensors provide measurements of the depth-weighted apparent electrical conductivity~~,~~ EC_a~~,~~ accordingly to the specific ~~depth~~ distribution of the ~~soil~~ bulk electrical conductivity~~,~~ σ_b~~,~~ as well as the depth response function of the sensor used (McNeill 1980). Thus, the dependence on σ_b makes EC_a sensitive to soil salinity and water ~~content~~distributions. In principle, specific procedures for estimating salinity and water content may be developed through controlled laboratory experiments where σ_b, σ_w and θ are measured simultaneously (Rhoades and Corwin 1981). That said, to monitor salinity and water content, it is crucial to correctly infer the depth-distribution of σ_b from profile-integrated EC_a readings.

To date, this issue has been tackled by applying two different strategies: The first is to use empirical calibration relations relating the depth-integrated EC_a readings to the σ_b values measured by alternative methods - like Time-Domain Reflectometry (TDR) - within discrete depth intervals (Rhoades and Corwin 1981, Lesch et al. 1992, Triantafilis, Laslett, and McBratney 2000, Amezketa 2006, Yao and Yang 2010, Coppola et al. 2016); The second consists in the 1D inversion of the observations from the EMI sensor to reconstruct the vertical conductivity profile (Borchers, Uram, and Hendrickx 1997, Hendrickx et al. 2002, Santos et al. 2010, Lavoué et al. 2010, Mester et al. 2011, Minsley et al. 2012, Deidda, Fenu, and Rodriguez 2014, ~~von Hebel et al. 2014~~Von Hebel et al. 2014).

With regard to EC_a inversion, a forward model still commonly used is the cumulative response model or local-sensitivity model (LSM) (McNeill 1980). McNeill's linear approach is well suited to the cases characterized by an induction number~~,~~ ~~β~~ B (defined as the ratio between the coil distance and the skin depth)~~,~~ much smaller than 1. However, because of the increasing computing power, improved forward modeling algorithms based on more accurate nonlinear approaches are becoming increasingly common (Hendrickx et al. 2002, Deidda, Fenu, and Rodriguez 2014, Deidda, Bonomi, and Manzi 2003, Lavoué et al. 2010, Santos et al. 2010). For example, these more sophisticated forward modeling codes can cope with a wider range of conductivities for which the assumption ~~β~~B<<1 is not necessarily met.

To obtain reliable vertical distributions of electrical conductivity, the EC_a data used for the inversion should consist of multi-configuration data. Hence, data collection should be performed either with the simultaneous use of different sensors or with different acquisition configurations with only one sensor (different configurations may consist, e.g., in different coil orientations, varying intercoil separations and/or frequencies – see, for example Díaz de Alba and Rodriguez, ~~(~~2016~~)~~). Multi-configuration data can be effectively used to invert for vertical electrical conductivity profiling since the EC_a measures actually investigate different, overlapping soil volumes. Devices specifically designed for the simultaneous acquisition of multi-configuration data are currently available. Some of them consist of one transmitter and several receivers with different coil separations and orientations (Santos et al. 2010). If, instead, a sensor with~~ a~~ single intercoil distance and frequency is available, a ~~valid~~ possible alternative to having multi-configuration measurements could be to record the data at different heights above the ground.

Unfortunately, like every other physical measurement, frequency-domain electromagnetic measurements are sensitive to noise that is very hard to model effectively. ~~Therefore~~Moreover~~, for example,~~ as discussed~~-~~, for example, in Lavoué et al. (2010), Mester et al. (2011), and ~~von Hebel et al. (2014)~~Von Hebel et al. (2014), an instrumental shift in conductivity values could be observed due to system miscalibration and the influence of surrounding conditions such as temperature, solar radiation, power supply conditions, the presence of the operator, zero-leveling procedures, cables close to the system and/or the field setup (see, amongst others, ~~(~~Sudduth, Drummond, and Kitchen 2001;~~,~~ Robinson et al. 2004;~~,~~ Abdu, Robinson, and Jones 2007;~~,~~ Gebbers et al. 2009;~~,~~ Nüsch et al. 2010). ~~Therefore~~ Hence, the EC_a data from EMI measurements would generally ~~need~~ require a proper calibration. One option could be to use soil cores as ground-truth data. In this case, EC_a measurements at the sampling locations ~~are~~ can be compared against EC_a data predicted by the theoretical forward response applied to the true electrical conductivity distribution measured directly on the soil cores (Triantafilis, Laslett, and McBratney 2000, Moghadas et al. 2012). Clearly, this strategy is extremely time- (and resource-) consuming. To avoid drilling, Lavoué et al. (2010) introduced a calibration method, later also adopted by Mester et al. (2011) and ~~von Hebel et al. (2014)~~Von Hebel et al. (2014), using the electrical conductivity distribution obtained from Electrical Resistivity Tomography (ERT) data as input for electromagnetic forward modeling. The EC_a values predicted on the basis of ERT data were used to remove the observed instrumental shift and correct the measured conductivity values by linear regression.~~-~~ However, in general, a prerequisite for such an approach concerns the reliability of the inversion of the ERT result. This is not only due to the quality of the original data, but also the adopted inversion procedure.

Indeed, ERT inversion is an ill-posed problem: its solutions are characterized by non-uniqueness and instability with respect to the input data (Yu and Dougherty 2000;~~,~~ Zhdanov 2002;~~,~~ Günther 2011). In the Tikhonov regularization framework, ill-posedness is addressed by including the available prior information. Such information can be very general. For example, it can be geometrical (i.e., associated to the presence of smooth or sharp boundaries between different lithologies). ~~Clearly~~Obviously, the final result largely reflects the initial guess formalized via the chosen regularization term (Pagliara and Vignoli 2006;~~,~~ Günther 2011;~~,~~ Vignoli, Deiana, and Cassiani 2012;~~,~~ Fiandaca et al. 2015).

When relatively shallow depths have to be explored (1-2m), direct soil sampling and ERT can be effectively replaced by TDR observations. TDR devices are designed to measure the dielectric properties of soils. More precisely, they measure the apparent electrical permittivity, from which, not only the dielectric constant, but also the effective electrical conductivity can be deduced (e.g., Dalton et al. 1984; Topp et al. 1988; Weerts et al. 2001; Noborio 2001; Jones et al. 2002; Robinson et al. 2003; Lin et al. 2007; Thomsen et al. 2007; Huisman et al. 2008; Lin et al. 2008; Koestel et al. 2008; Bechtold et al. 2010). In general, TDR measurements might be difficult to be used to recover the electrical conductivity with the desired accuracy. However, in the literature, many examples are reported in which, within the range 0.002 – 0.2 S/m (compatible with the examples investigated in the present research), and by properly using the TDR device (e.g., by paying attention to minimize the effects of nonparallel device rods inserted into the ground), the TDR conductivity can be measured with an uncertainty level lower than 5% (e.g.: Huisman et al., 2008; Bechtold et al., 2010). Besides, since the TDR measurements are commonly calibrated in saline solutions just before the field data acquisitions, they could potentially provide a reliable, absolute estimation of the actual ground conductivity (Ferré et al., 1998a). For this reason, in some cases, TDR observations have been proposed as a valid tool for ground-truthing the ERT and, possibly, as ancillary information source to constraint for the ERT inversions (Koestel et al. 2008). For additional studies dealing with the use of ERT data for the validation of the EMI and TDR measurements for soil characterization we refer the reader to, for example, Cassiani et al. 2012 and Ursino et al. 2014.

In th~~is line of reasoning, ~~e present research, we~~this paper~~ focus~~es~~ on the use of TDR data to absolute calibrate ~~EC$_a$~~ the conductivities ~~measurements~~ obtained ~~via~~ by inverting the EMI measurements. To do this, a dataset collected during an experiment carried out along four transects under different salinity and water content conditions (and monitored ~~by~~ with both EMI and TDR sensors) ~~will~~ is ~~be~~ utilized. We first tackle the problem of inferring the soil electrical conductivity distribution from multi-height EC$_a$ readings via the proper inversion strategy. Then we assess the quality of these reconstructions by using TDR data as ground-truth. In this respect, in the following, we discuss how to effectively compare the σ_b values generated by the EMI inversion with the associated TDR values. In fact, as discussed by ~~(~~Coppola et al. 2016~~)~~, because of their relatively smaller observation volume, TDR data provide quasi-pointlike measurements and do not integrate the small-scale variability (of soil water content, solute concentrations, etc.) induced by natural soil heterogeneity. By contrast, EMI data necessarily overrule the small-scale heterogeneities seen by TDR probes as they investigate a much larger volume. Accordingly, the paper provides a methodology to calibrate EMI results by TDR readings. This procedure lies in conditioning the original TDR data and in the statistical characteristics of the two EMI and TDR data series. On the basis of the proposed analysis, we discuss the physical reasons for the differences between EMI and TDR-based bulk electrical conductivity and identify a method to effectively ~~transfer~~ migrate the reliable TDR information across the larger volume investigated by EMI.

Materials and Methods

The experiment was carried out at the Mediterranean Agronomic Institute of Bari (MAIB) in south-eastern Italy. The soil was pedologically classified as Colluvic Regosol, consisting of a silty-loam layer of an average depth of 0.6 m on fractured calcarenite bedrock. The experimental set-up (~~Figure~~ Fig. 1) consisted of four transects of 30 m length and 2.8 m width, equipped with a drip irrigation system with five dripper lines placed ~~at~~ 0.35 m ~~distance~~ apart and characterized by an inter-dripper distance ~~among drippers along each line~~ of 0.2 m. The ~~,~~ ~~with a~~ dripper discharge was ~~of~~ 2 l/h. Green beans were grown in each transect. The irrigation volumes were calculated according to the time-dynamics of water content in the first 0.25 m measured by a TDR probe inserted vertically at the soil surface. TDR readings were taken: (i) just before and (ii) two hours after every irrigation. Based on the difference between the water content at field capacity and that measured just before irrigation, it was easy to assess the volumes needed to bring the soil water content back to the field capacity ~~were able to be calculated~~.

The four transects were irrigated with water at two different salinity levels and with two different water volumes. Transect 1: 100% of the irrigation water at 1 dSm^{-1} (hereafter 100-1dS); Transect 2: 50% of irrigation water at 1 dSm^{-1} (50-1dS); Transect 3: 100% of the irrigation water at 6 dSm^{-1} (100-6dS); Transect 4: 50% of irrigation water at 6 dSm^{-1} (50-6dS). Water salinity was induced by adding calcium chloride ($CaCl_2$) to tap water. Irrigation volumes were applied every two days.

EMI readings - in ~~both horizontal (EC_aH) and~~ vertical magnetic dipoles ~~(EC_aV)~~ configurations - were collected by using a Geonics EM38 device (Geonics Limited, Ontario, Canada). The EM38 operates at a frequency of 14.6 kHz with a coil spacing of 1 m, and with ~~an effective~~a nominal measurement depth of ~~≈0.75 m and~~ ~≈1.5 m~~, respectively,~~ ~~in the horizontal and vertical dipole configurations~~ (McNeill, 1980). The lateral footprint of the EM38 measurement can be considered approximately equal to the vertical one. Thus, the σ_b seen by the EMI, in a given ~~discrete~~ depth-layer, necessarily differs from that seen by a TDR probe ~~in~~ at the same depth-layer, due to the very different spatial resolutions.

At the beginning of ~~each~~ the measurement campaign, the EMI sensor was "nulled" according to the manufacturer's manual. Readings were taken just after each irrigation application at 1 m step, along the central line of each transect, for an overall total of 26 ~~measurements~~ soundings per transect~~, per campaign~~. Multi-height EM38 readings were acquired at heights of 0.0, 0.2, 0.4 and 0.6 m from the ground. Taking measurements just after irrigation allowed relatively time-stable water contents to be assumed at each site throughout the monitoring ~~campaigns~~phases.~~.~~

~~Multi-height EM38 readings were performed at 26 locations in the middle line of each transect during the growing season. Readings were acquired at heights of 0.0, 0.2, 0.4 and 0.6 m from the ground. Overall, seven EM38 measurement campaigns were carried out during the experiment, from July 7th to September 2nd.~~

Just after ~~each~~ the EM38 measurements~~ campaign~~, a TDR probe was inserted vertically at the soil surface ~~(0.0-0.25 m)~~ in 26 ~~sites~~locations, each corresponding to the central point of an EM38 reading. A Tektronix 1502C cable tester (Tektronix Inc., Baverton, OR) was used in this study. It enables simultaneous measurement of water content~~,~~ θ~~,~~ and bulk electrical conductivity~~,~~ σ_b~~,~~ of the soil volume explored by the probe (Heimovaara et al. 1995;~~,~~ Robinson and Friedman 2003~~,~~; Coppola et al. 2011~~,~~; Coppola et al. 2015). The TDR transmission line consisted of an antenna cable (RG58, 50 Ω characteristic impedance, 2 m long and with 0.2 Ω connector impedance) and three-wire probes, 0.25 m long, 0.07 m internal distance, and 0.005

m in diameter. The TDR probe was not embedded permanently at fixed depths along the soil profile to avoid any potential disturbance to the EMI acquisitions.

~~Only ~~T~~immediately after the last EM38 campaign (September 2nd) ~~he ~~were ~~TDR readings were taken at three different depth intervals (0.0-0.2, 0.2-0.4, 0.4-0.6 m). After the measurements at the surface (0.0-0.2 m), a trench was dug up to 0.2 m depth. TDR probes were then inserted vertically for the additional collection of the data in the interval 0.2-0.4 m, after which the trench was deepened up to 0.4 m and readings were taken at 0.4-0.6 m. The $\sigma_{b,TDR}$ readings ~~in this last campaign ~~were used for the calibration of the EM38 ~~data~~inversion results.~~ All the remaining six data series will be used for a validation study of the approach developed in this paper (which will be the subject of a follow-up paper).~~

Data Handling

Multi-height EMI readings inversion

Nonlinear 1D forward modeling, which predicts multi-height EMI readings from a loop-loop device, can be obtained by suitable simplification of Maxwell's equations that takes the symmetry of the problem into account. This approach is described in detail in (Hendrickx et al. 2002), and is based on a classical approach extensively described in the literature (Wait 1982~~,~~; Ward and Hohmann 1988). The predicted data are functions of the electrical conductivity and the magnetic permeability in ~~a homogeneously and~~a horizontally layered medium.

When the coils of the recording device are vertically oriented with respect to the ground surface, the reading at height *h* can be expressed by using the integral:

$$-\rho^3 \int_0^\infty \lambda^2 e^{-2h\lambda} R_0(\lambda) J_0(\rho\lambda)\, d\lambda, \tag{1}$$

where ρ denotes the distance between the coils, $J_0(\lambda)$ is the Bessel function of the first kind of order 0, and $R_0(\lambda)$ is a complex valued function which depends upon the electromagnetic properties of the ground layers. A similar expression is valid also when the coils are horizontally aligned. Hence the dependence of the measured data on the electrical conductivity σ_k, of the (homogeneous) j-th layer is incorporated into the function $R_0(\lambda)$. We discretize the problem with n layers whose characteristic parameters σ_j (with j = 1, . . ., n) are the unknowns we invert for. In the present research, we neglect any dependence of the electromagnetic response on magnetic permeability as we assume it is fixed and equal to the permeability of empty space. ~~We~~ In principle, it is possible to consider two measurements for each location: one for the horizontal and one for the vertical configuration of the transmitting and receiving loops. In this ~~way~~case, the data used as inputs for the inversion are 2*m, where m is the number of heights $h_1, h_2, \ldots, h_m$ where the measurements are performed.

A least squares data fitting approach leads to the minimization of the function:

$$f(\sigma) = \frac{1}{2}\sum_{i=1}^{2m} r_i^2(\sigma), \tag{2}$$

where $\boldsymbol{\sigma} = (\sigma_1, \ldots, \sigma_n)^T$, and $r_i^2(\sigma)$ is the misfit between the *i-th* measurement and the corresponding forward modeling prediction based on ~~equation (1)~~Eq. 1.

We solve the nonlinear minimization problem by the inversion procedure described in Deidda, Fenu, and Rodriguez (2014). The algorithm is based on a damped regularized Gauss-Newton method. The problem is linearized at each iteration by means of a first order Taylor expansion. The use of the exact Jacobian (whose expression is detailed in Deidda, Fenu, and Rodriguez, ~~(~~2014) makes the computation faster and more accurate than using a finite difference approximation. The damping parameter is determined in order to ensure both the convergence of the method and the positivity of the solution. The regularized solution to each linear subproblem is computed by the truncated generalized singular value decomposition (TGSVD - Díaz de Alba and Rodriguez, ~~(~~2016) employing different regularization operators. Besides the classical regularization matrices based on the discretization of the first and second derivatives, to further improve the spatial resolution of EMI inversion results in all the cases characterized by sharp interfaces, we tested a nonlinear regularization stabilizer promoting the reconstruction of blocky features (Zhdanov, Vignoli, and Ueda 2006~~,~~; Ley-Cooper et al. 2015~~,~~ ; Vignoli et al. 2015~~,~~ ; Vignoli et al. 2017). The advantage of this relatively new regularization is that, when appropriate prior knowledge about the medium to reconstruct is available, it can mitigate the smearing and over-smoothing effects of the more standard inversion strategies. This, in turn, can make the calibration of the EMI data against the TDR data more effective. For this reason, in the following, the EMI results used for our assessments are those inferred by means of this sharp ~~regularization~~inversion. The differences between the “standard” smooth (based on the first derivative) reconstruction and the sharp one are clearly shown in ~~Figure~~ Fig.s 2 and 4. In all cases, the inversions are performed with a 100-layer homogeneous discretization, down to 8 m, with fix interfaces. We opted for such a parameterization to be able to: (i) control the inversion results by acting merely on the regularization parameters, and (ii) remove the regularization effects possibly originated by the discretization choice (e.g., the number of layers, interfaces locations). In this way, it was possible to use an automatic strategy for the selection of the regularization parameters.

In Fig.s 2 and 4, the sharp results (upper panels) associated with the cases 100-6dS and 50-6dS are compared against the corresponding smooth inversions (middle panels). Even if the data misfit levels largely match (lower panels in Fig.s 2 and 4, but also Fig.s 3 and 5), the two inversion strategies produce reconstructions that differ significantly. This is due to the inherent ill-posedness of the EMI inversion. By considering solely the geophysical observations, it is impossible to decide which model is the best. In this research, based on the fact that, just after the irrigation, the effect of the water is supposed to remain localized in the shallowest portion of the soil section, the sharp inversion was found to provide more reliable results. Moreover, to some extent, the general better agreement of the data calculated from the sharp model supports the idea that the electrical properties distributions are better inferred via the sharp regularization. In any case, since in this research we calibrate the EMI-derived models (and not the data), the final calibrated result will reflect the assumptions made in the first place when the EMI data are inverted (specifically, the regularization assumptions).

A possible alternative way to still effectively use the TDR data to calibrate the EMI measurements (and not the associated conductivity model) could consist in performing the calibration in the data-space (and not in the model-space). In this case, the measured TDR conductivity could be used as input model to calculate the EC_a response of the EMI device actually used. In turn, this calculated EC_a response can be compared against the measured EMI data and used for their calibration. However, eventually, also this latter data-space calibration will have to deal with the inversion issues once the calibrated EMI data need to be converted into conductivities σ_b. In this paper, we chose the model-space calibration strategy as, in general, in the available EMI inversion codes, it is not always easy to decouple the forward modelling routines from the overall inversion algorithm. Hence, the discussed approach could be more directly applicable and beneficial for practitioners. On the other hand, it is true that the data-space calibration naturally takes into account the scale-mismatch between the TDR and the EMI measurements with no need for any statistical calculation.

It is worth noting that the constant magnetic permeability assumption is not always valid.~~:~~ I~~i~~nverting for the magnetic permeability is sometimes not only necessary, but it can also provide an additional tool for soil characterization (e.g., Beard and Nyquist, 1998; Farquharson, Oldenburg, and Routh, 2003; Deidda, Diaz De Alba, and Rodriguez 2017).

For the sake of clarity, hereafter, the σ_b values generated from the EMI data inversion will be identified explicitly as $\sigma_{b,EMI}$.

TDR-based water content and bulk electrical conductivity

The Tektronix 1502C can measure the total resistance~~,~~ R_t~~,~~ of the transmission line by:

$$R_t = Z_c \frac{(1+\rho_\infty)}{(1-\rho_\infty)} = R_s + R_c \tag{3}$$

where: R_s is the soil's contribution to total resistance and R_c accounts for the contribution of the series resistance from the cable;~~,~~ the connector~~,~~ Z_c~~,~~ is the characteristic impedance of the transmission line;~~,~~ and ρ is a reflection coefficient at a very long time, when the waveform has stabilized.

The σ_b value at 25°C can be calculated as (Rhoades and van Schilfgaarde 1976~~,~~; Wraith et al. 1993):

$$\sigma_{b\,25^\circ C} = \frac{K_c}{Z_c} f_T \tag{4}$$

where K_c is the geometric constant of the TDR probe and f_T is a temperature correction factor to be used for values recorded at temperatures other than 25°C. Both Z_c and K_c can be determined by measuring R_t with the TDR probe immersed in a solution with known conductivity σ_b. Hereafter, these σ_b measurements will be identified as $\sigma_{b,TDR}$.

Evaluation of Concordance between $\sigma_{b,TDR}$ measurements and $\sigma_{b,EMI}$ estimates

The agreement between $\sigma_{b,TDR}$ measurements and $\sigma_{b,EMI}$ estimations in the 0.0-0.~~20~~ 6 m ~~layer~~ range was evaluated by the Concordance Correlation Coefficient, ρ_L :

$$\rho_L = \frac{2s_{xy}}{z_x^2 + z_y^2 + (m_x - m_y)^2} \tag{5}$$

where m_x, m_y, s_x, s_y, s_{xy} are means, standard deviations and covariances of the two data series ($x = \sigma_{b,EMI}$; $y = \sigma_{b,TDR}$), respectively.

Scatter plots of the $\sigma_{b,EMI}$ and $\sigma_{b,TDR}$ data series (both original and filtered) ~~for the depth interval 0.0-0.20 m~~ were evaluated by the line of perfect concordance (1:1 line) and the reduced major axis of the data (RMA) (Freedman et al. 1991). The method combines measurements of both precision and accuracy to determine how close the two data series are to the line of perfect concordance $\sigma_{b,EMI} = \sigma_{b,TDR}$. Compared to the classical Pearson correlation coefficient, ρ_P:

$$\rho_P = \frac{s_{xy}}{s_x s_y}, \tag{6}$$

ρ_L not only measures the strength of linear relationship (how close the data in the scatter plot are to a line), but also the level of agreement (how close that line is to the line of perfect agreement, the 1:1 line). In this sense, ρ_L may also be calculated as (Cox 2006):

$$\rho_L = \rho_P C_b,$$

$$C_b = \frac{2}{(v + 1/v + u^2)}, \tag{7}$$

$$v = s_x / s_y,$$

and

$$u = (m_x - m_y)/\sqrt{s_x s_y},$$

where C_b is the bias correction factor measuring how far the best-fit line deviates from the 1:1 line. The maximum value of C_b = 1 (0<C_b<1) corresponds to no deviation from the line. The smaller C_b is, the greater the deviation from the line. In other words, C_b is a measure of accuracy (how much the average estimate differs from the average measurement value, assumed to be the true value) and refers to the systematic error, whereas ρ_P is a measure of precision (measures the variability of measurements around their own average) and refers to the random error. The RMA line is given by:

$$y = \left(m_y - \beta m_x\right) + \beta x = \alpha + \beta x. \tag{8}$$

This line passes through the means of the x and y values and has slope given by the sign of Pearson's correlation coefficient, ρ_P, and the ratio of the standard deviations, s, of the two series (Freedman et al. 1991, Corwin and Lesch 2005):

$$\beta = s_y / s_x . \tag{9}$$

ρ_L increases in value as (i) the RMA approaches the line of perfect concordance (a matter of accuracy) and (ii) the data approach the RMA (a matter of precision). In the ideal case of perfect concordance, the intercept of the RMA, α, should be 0 and β should be 1. Therefore, α ≠ 0 or β ≠ 1 indicate additive and/or multiplicative biases (location and/or scale shifts). The concordance was evaluated for the original TDR data, as well as for the filtered TDR data. For the analysis ~~carried out in the results section~~described in detail later in the paper, it is worth noting ~~here~~ that the coefficients α and β depend only on the statistical characteristics (mean and standard deviation) of the two series, as $\alpha = m_y - \beta m_x$ and $\beta = s_y / s_x$.

Fourier filtering

Because of their relatively small observation volume (~~≈~~~10^{-3} m^3), TDR sensors provide quasi-pointlike measurements and are, thus, more effective in capturing small-scale variability (in water content, solute concentrations) induced by natural soil heterogeneity. Thus, the variability within a set of TDR readings is expected to originate from a combination of small and large-scale heterogeneities (high and low spatial frequency components). By contrast, the EMI measurements (because of the size and physics of the instrumentation) necessarily integrate out the small-scale variability at the TDR scale of investigation.

Hence, in order to make the two datasets comparable, the original spatial TDR data series need to be filtered to remove the variation from small-scale heterogeneities (recorded only by the TDR probe). In this way, only the information at a spatial scale equal to or larger than the observation volume of both sensors is preserved.

Thus, a simple filter based on the Fourier Transform (FT) is applied to the TDR series. ~~The Fourier transform (FT) of discrete stationary series of length M equispaced at intervals Δp (x_p, p=0,1,…,M-1) (where x is the variable, and p the spatial or temporal location on the series) is defined as (Shumway 1988):~~

$$\cancel{X(k)=M^{-1}\sum_{s=0}^{M-1}\left(x_p-\bar{x}\right)\exp\left(-2\pi i v_k p\right),} \qquad \cancel{(10)}$$

~~where k= 0,1….,M-1, X(k) are the Fourier coefficients, i=$\sqrt{-1}$, v_k= k/M is the wave number (or frequency) in cycles per unit distance (or time) and $\bar{x}$ is the sample mean. If the series is detrended, x_p in equation (22) is the detrended series.~~

~~The FT in equation (10) may be written in terms of sine and cosine transform, noting that:~~

$$\cancel{\exp\left(-2\pi i v_k p\right)=\cos\left(-2\pi v_k p\right)-i\sin\left(-2\pi v_k p\right)} \qquad \cancel{(11)}$$

~~Thus equation (10) becomes:~~

$$\cancel{X(k)=X_C(k)-iX_S(k)} \qquad \cancel{(12)}$$

~~The Fourier coefficients X(k) are complex numbers. Most software packages (e.g., MatLab, SAS, Microsoft Excel) have built-in Fast Fourier transform (FFT) algorithms that considerably speed~~

~~up the computation of equation (10); the sine and cosine transforms are immediately available from the real and imaginary parts of the computed X(k).~~

~~By using the following coefficients:~~

$$a_k = -\frac{2}{M}\mathrm{imag}(X(k)), \quad 0 < k < \frac{M}{2};$$
$$b_k = -\frac{2}{M}\mathrm{real}(X(k)), \quad 0 < k < \frac{M}{2}, \qquad (13)$$

~~it is easy to perform the inverse FT and recover the original signal:~~

$$x(p) = a_0 + \sum_{k=0}^{(M-1)/2}\left(a_k \sin(2\pi \nu_k p) + b_k \cos(2\pi \nu_k p)\right) \qquad (14)$$

~~Equation (14) is central to the filtering approach we use in the present paper. It can be used to reconstitute a smoothed data series by retaining selected harmonics alone (e.g., only the low frequency harmonics). The frequencies to be selected can be identified by examining the power spectral density - see equation (16) below - of the data series.~~

~~The periodogram can be written as the squared modulus of the FT:~~

$$P_x(\nu_k) = |X(k)|^2 = \left[X_C^2(k) + X_S^2(k)\right] = X(k)\overline{X(k)}, \qquad (15)$$

~~where the overbar denotes complex conjugate.~~ P_x ~~is an asymptotically unbiased estimator for the spectrum (Shumway 1988). It is common practice to average adjacent values of the periodogram to obtain estimates with more degrees of freedom, and create a smoothed power spectrum. The average spectral estimator, in a frequency interval centered on~~ ν_k, ~~is defined as:~~

$$f_x^{P,B}(\nu_k) = L^{-1}\sum_{l=-(L-1)/2}^{(L-1)/2} P\left(\nu_k + \frac{l}{M}\right) = L^{-1}\sum_{l=-(L-1)/2}^{(L-1)/2} |X(k+l)|^2, \qquad (16)$$

~~where L is some odd integer considerably smaller than M and defining the size of the averaging window. Hence, the averaging window is characterized by a bandwidth B = L/M (cycles per point) centered on~~ ν_k. $f_x^{P,B}(\nu_k)$ ~~is the periodogram-based power spectrum averaged on B and~~

~~with, approximately, a chi-squared distribution, in which the degrees of freedom depend on the width L of the window used.~~

~~The 100(1-α) confidence interval for the smoothed spectrum can be calculated as:~~

$$\frac{2Lf_x^{P,B}(\nu_k)}{\chi^2_{2L}(a/2)} \le f_x^n(\nu_k) \le \frac{2Lf_x^{P,B}(\nu_k)}{\chi^2_{2L}(1-a/2)}, \qquad (17)$$

So, a low-pass frequency filtering is performed on the TDR data to remove all components related to the small scale heterogeneities and make it comparable with the EMI measurements. More specifically, for each transect, we consider the $\sigma_{b,EMI}$ reconstruction and, for each of its 1D models, calculate the average conductivity value within each depth interval for which the TDR data are available (namely: 0.0-0.2 m, 0.2-0.4 m, 0.4-0.6 m). Hence, for each depth interval, along the entire transect, we can calculate the mean and standard deviation of the conductivity values retrieved from the EMI observations. Subsequently, this standard deviation (associated with the EMI data) is compared with the standard deviation of the iteratively low-pass filtered TDR data for the same depth interval. In this way, an optimal cut-off frequency can be selected to make the scales of the two kinds of measurements compatible. Figure 6 shows the comparison between the standard deviations of the EMI and filtered TDR data, for the 50-6dS transect, at 0.2-0.4 m depth. In this specific case, the selected cut-off frequency to filter the TDR data is 0.313 cycles/m, corresponding to a 3.2 m range. This is not surprising at this is of the order of magnitude of the footprint of the EMI measurements. ~~where α is the significance level and $f_x^n(\nu_k)$ is the background noise power spectrum. The null hypothesis is $f_x^{P,B}(\nu_k) = f_x^n(\nu_k)$ vs. $f_x^{P,B}(\nu_k) \ne f_x^n(\nu_k)$. If $f_x^n(\nu_k)$ falls within the interval in equation (17), we fail to reject the hypothesis. If not, the estimated power spectrum at a given frequency ν_k has to be considered significantly different from that of the assumed background noise. In the case of~~

~~white noise, implying a uniform distribution of the power spectrum across frequencies,~~ $\cancel{f_x^n(\nu_k)}$ ~~can be considered as the mean of all power spectrum estimates.~~

Results and Discussion

Hereafter, the original and filtered data will be respectively labeled ORG and FLT. The graphs on the top panels ~~in panel (a) of~~ in ~~Figures~~ Fig. ~~3, 4 and 5~~7 compare $\sigma_{b,TDR}$ measured by TDR against the corresponding conductivity $\sigma_{b,EMI}$ retrieved by the EMI (sharp) inversion~~,~~ ~~respectively,~~ for the all the transects~~layers at 0-0.20, 0.20-0.40, and 0.40-0.60 m~~. From the left, the graphs refer respectively to the transects identified as 100-6dS, 50-6dS, 100-1dS and 50-1dS. All ~~the~~ plots show the data for the entire investigated profile between 0.0 and 0.6 m, together with the line of perfect concordance (1:1, black line), and the main regression axis (MRA, red line)~~report the line of perfect concordance (1:1, black line) and the main regression axis (MRA, red line)~~.

The general ~~outcome~~ conclusion is that, in all four transects, and for all three considered depth-layers, the $\sigma_{b,EMI}$ values underestimate the $\sigma_{b,TDR}$ measurements, such that the MRA line generally lies above the 1:1 line. Not surprisingly, the EMI result seems quite insensitive to TDR variability. Also, a considerable scatter around the MRA line may be observed for all ~~four~~ transects.

Table~~s~~ 1~~, 2 and 3~~ shows the MRA coefficients (C_b, α , β), as well as the Pearson, ρ_P, and the concordance correlation, ρ_L, for the three depth-layers and for all four transects investigated. We recall that the bias correction factor~~,~~ C_b, the slope~~,~~ β, and the intercept~~,~~ α~~,~~ should be respectively close to 1, 1 and 0, for the MRA to approximate the line of perfect concordance. For all the transects and all the depth-layers considered, the parameters confirm the relatively loose relationship between $\sigma_{b,EMI}$ and $\sigma_{b,TDR}$ already observed in the graphs, both in terms of accuracy (the distance of the MRA line from the 1:1) and precision (the data scatter around the MRA line).

V~~v~~on Hebel et al. (2014) found a similar behavior when comparing their EMI and ERT datasets. In that case, the EC_a values measured by EMI systematically underestimated the EC_a generated by applying EMI forward modeling to the σ_b distribution retrieved by ERT. To remove the bias, the authors ~~simply~~ performed a linear regression between measured and predicted EC_a after applying a ten-term moving average to the original data. By using the regression coefficients, all the measured EC_a values were converted to ERT-calibrated EC_a values.

Here, we follow a different approach to calibrate the $\sigma_{b,EMI}$ values against the $\sigma_{b,TDR}$ measurements based on the MRA coefficients and, ~~hence~~ so, on the statistical parameters (mean and standard deviation) of the two data series. Specifically, the present approach looks for a systematic correction of the bias based on well-defined statistical sources of the discrepancies. In short, the proposed method performs the calibration in the σ_b model-space, instead of the EC_a data-space.

Our model-space approach mostly relies on the statistical parameters of the two series. Analyzing the role of these statistics in explaining the discrepancies between EMI and TDR data observed in ~~Figures 3-5~~Fig. 7a may help to understand how they can be effectively ~~exploited~~ used for ~~converting~~ making EMI ~~measurements~~ results directly comparable ~~to~~ with the TDR values.

In nearly all of the graphs in the top panels ~~(a) of~~in Fig.~~ures~~ ~~3-5~~7, the discrepancies between $\sigma_{b,EMI}$ and $\sigma_{b,TDR}$ values can be decomposed in the following components:

1. The distance along the $\sigma_{b,EMI}$ axis of the MRA line from the 1:1 line, that is the difference between the $\sigma_{b,EMI}$ and the $\sigma_{b,TDR}$ means.

2. The difference in the slope of the MRA and of the 1:1 lines, which stems from the different variability of $\sigma_{b,EMI}$ (its standard deviation) and that of $\sigma_{b,TDR}$. We recall here that the slope of the MRA is just the ratio of the two standard deviations, $\hat{\beta} = s_y / s_x$.

3. The scatter of the data around the MRA line, which may come from different sensors' noise and the influence of surrounding conditions (e.g., temperature).

Below, we analyze in detail the role of all these three points with the support of the measured data.

1. The distance of the MRA from the 1:1 line ~~may~~ is ~~be~~ mostly ~~ascribed~~ due to the difference in the observed means. The ~~graph~~ plot in Figure ~~6a~~ 8a compares the means for the two original series (~~open~~ squares-solid line for TDR, ~~open~~ circles-dashed line for EMI). ~~The plot in~~ Figure 8~~6~~b reports the same comparison on a 1:1 plot (~~open~~ triangles-solid regression line). The mean values~~s~~ confirm the general underestimation of TDR by the EMI data. However, the trends are evidently similar, which is reflected in the high correlation between the means of the two series, with a significantly high R^2=0.81. ~~The~~ This high correlation ~~of the means~~ has very positive implications from an applicative point of view, ~~as~~since, after the calibration in a specific ~~soil~~site, it allows the ~~TDR~~ EMI mean to be inferred given the mean of ~~EMI~~ TDR readings taken in that soil, and thus ~~gives us~~provides the possibility to ~~transpose~~ migrate the more reliable TDR information across the larger area that can be practically investigated ~~with~~ during an EMI survey.

2. The different slope of the two lines has to be ascribed to the different variability of the two series. ~~The graph in~~ Figure ~~7a~~ 9a compares the standard deviations for the two original series (~~open~~ squares-solid line for TDR, ~~open~~ circles-dashed line for EMI). ~~The graph in f~~Figure ~~7b~~ 9b reports the same comparison on a 1:1 plot (~~open~~ triangles-solid regression line). Conceptually,

the different variability of the two series ~~may~~can ~~well~~ be related to the different sensor observation volumes (~~coming~~ originated from the different spatial sensitivity of the sensors~~)~~ - ~~(~~Coppola et al. 2016). For TDR probes, most of the measurement sensitivity is close to the rods (~~Ferre et al. 1998~~Ferré et al. 1998b). Conversely, the spatial resolution of inverted EMI EC_a values may be much lower as the resolution of the EMI result depends on the physics of the method, the specifications (and configuration) of the recording device, and the regularization ~~type~~ strategy applied during the inversion. ~~That said~~Thus, the EMI is generally unable to capture the small-scale variability seen by the TDR. For our calibration purposes, it is important to make the variability of EMI and TDR conductivities actually comparable. As discussed by Coppola et al., ~~(~~2016~~)~~, a possible method can ~~be~~ consist in ~~to~~ filtering out ~~-~~the high frequency components (at small spatial scale) of the original TDR data, while retaining the lower frequency information. This corresponds to keep~~,~~ ~~that is~~ the information at a spatial scale larger than the observation volume of the TDR sensor and attuned with the resolution of the $\sigma_{b,EMI}$ ~~EMI~~ distribution~~ values coming from the inversion~~. From a practical point of view, this makes sense, as TDR readings are often "too local" to actually represent the macroscopic physical characteristics of interest for applications (water content, solute concentrations). The volume explored by a TDR probe may, or may not, include preferential channels (Mallants et al. 1994;~~,~~ Oberdörster et al. 2010), stones (Coppola et al. 2011~~,~~; Coppola et al. 2013), small-scale changes in the texture and structure (Coppola et al. 2011), which can make the interpretation of local measurements difficult for practical applications. In this sense, EMI's removal of these small-scale effects may be desirable from a management perspective.

~~Accordingly~~Consistently, the original TDR data ~~were~~ are conditioned via ~~Fourier~~ a low-pass filtering, as described in the Data Handling ~~Material and Methods~~ section. ~~The number of low-frequency harmonics to be used for rebuilding the filtered signal was selected according to the~~

~~spectrum for each depth and transect - see equation (16) - and, in general, it was included in three-six harmonics.~~ The filtering results, in terms of standard deviations, are reported in ~~figure~~ Fig. ~~7a~~ 9a (crosses-dashed line) and ~~in figure~~Fig. ~~7b~~ 9b (~~open~~ squares-dashed regression line). As expected, ~~filtering~~ the low-pass filter ~~made~~ makes the standard deviations much closer (almost overlapping ~~in many cases~~) ~~for~~ in all transects and ~~for~~ all considered depth-layers. The regression improved significantly from 0.25 for the original data to 0.78 ~~when~~ after the TDR data ~~were filtered~~filtering. ~~As with the means, the high correlation of the standard deviations has positive implications from a practical point of view: it allows the TDR standard deviation to be inferred, given the standard deviation of EMI readings taken in that soil. Panel b of Figures 3 to 5 shows the comparison of the original EMI and filtered TDR data. The concordance coefficients in the case of filtered TDR data are again reported in Tables 1 to 3. Obviously, because of the almost overlapping EMI and TDR standard deviations after filtering, the MRA line turned out to be much more parallel to the 1:1 line, as indicated by the coefficient β, which is now much closer to 1.~~

3. The scatter is consistently reduced by the spatial filtering (as similarly discussed in Von Hebel et al., 2014).

Eventually, the calibrated $\sigma_{b,EMI}^{rg}$ distribution (superscript *rg* means: EMI data after regression) can then be obtained from the original $\sigma_{b,EMI}$ via the linear mapping:

$$\sigma_{b,EMI}^{rg} = \alpha + \beta \sigma_{b,EMI} \quad (10)$$

where the coefficients α and β can be easily calculated from the means and standard deviations of the EMI results and the filtered TDR data. Thus, if m_{EMI} *and* $m_{TDR(FLT)}$, and s_{EMI}, and $s_{TDR(FLT)}$ are, respectively, the means and the standard deviations of the original $\sigma_{b,EMI}$ EMI data and of the filtered $\sigma_{b,TDR(FLT)}$ TDR data, the MRA line coefficients can be expressed as $\alpha = m_{TDR(FLT)} - \beta m_{EMI}$ and $\beta = s_{TDR(FLT)} / s_{EMI}$.

~~In general, however, filtering left the scatter around the MRA line almost unaltered. Here the scatter was zeroed by again using the intercept and the slope coefficients of the MRA obtained after TDR filtering. Specifically, the filtered TDR data were recalculated from the original EMI data as:~~

$$\cancel{\sigma^{rg}_{b,TDR(FLT)} = \alpha + \beta\sigma_{b,EMI}} \qquad \cancel{(18)}$$

The bottom panels in Fig. 7 show the results of the application of the linear mapping. In particular, they compare the calibrated EMI data (EMI rg) with the filtered TDR (TDR FLT) measurements. The MRA parameters and the concordance coefficients in the case of filtered TDR data are reported in Table 2. Clearly, considering the (calibrated) EMI and (filtered) TDR standard deviations turns the MRA line to be practically matching the 1:1 line, with the coefficient β approaching to 1. Moreover, from Table 2, the improvement of the bias C_b and the concordance ρ_L is generally significant. On the other hand, the Pearson's correlation ρ_P is not influenced by the recalibration as the proposed approach deals with the statistics of the data series rather than the single data. Thus, after the application of the low-pass filter to the TDR data, the coefficient β is close to 1, and the calibration turns out to be (almost) a simple shift of the inverted $\sigma_{b,EMI}$. The amount of this shift is equal to the difference between the mean values $m_{TDR(FLT)}$ and m_{EMI}. To summarize, the TDR filtering allows removing the outlier values generated by the small scale variability and preserving the information content necessary to properly calculate the shift required for the absolute calibration of the EMI inversion results.

Figure 10 shows, on the left, the original $\sigma_{b,EMI}$ distribution to be compared against the $\sigma^{rg}_{b,EMI}$

results (on the right) obtained through the application of the linear transformation in Eq. 10. The calibrated transects preserves the spatial variability of the original EMI inversions, but are now characterized by value ranges that are more realistic (as they are obviously closer to the TDR measurements assumed to be more representative of the real soil conditions).

~~The superscript *rg* means filtered data after regression. The results are again reported in panel c of figures 3-5. As an example of the calibration results, figure 8 compares the maps of bulk electrical conductivity for the 100-6dS transect obtained respectively by plotting the original $\sigma_{b,EMI}$ (figure 8a) coming from the inversion of the EMI signal and the calibrated $\sigma^{rg}_{b,TDR(FLT)}$ (figure 8b) obtained by applying the equation 18 to the $\sigma_{b,EMI}$ data of the first map. After calibration, the nearly homogeneous σ_b distribution represented in the map of figure 8a, coming from the substantial insensitivity of the original EMI data to TDR variability, turn into a physically more plausible σ_b layering, largely reproducing the true one observed by the TDR probes .~~

~~All the points discussed above provide the rationale to deduce the TDR-FLT data based on the statistical parameters of the EMI and TDR data (m_x, m_y, s_x, s_y). Summarizing, the procedure requires the following steps:~~

~~1. Filtering the TDR data, by retaining only the low-frequency part of the signal. The number of harmonics to be selected depends on the length of the data series, as well as on the spectrum characteristics. This step will make the standard deviations of the two data series similar, thus turning the data parallel to the 1:1 line;~~

~~2. Using the average (m_x, m_y) and the standard deviation (s_x, s_y) of the original $\sigma_{b,EMI}$ EMI data and of the filtered $\sigma_{b,TDR(FLT)}$ TDR data to calculate the MRA line coefficients as $\alpha = m_y - \beta m_x$ and $\beta = s_y / s_x$. Of course, the averages for the original and the filtered TDR data will coincide;~~

~~3. Straightening the data on the MRA line (zeroing the scatter) by recalculating the TDR-FLT data from the original EMI data and the MRA coefficients $\sigma^{rg}_{b,TDR(FLT)} = \alpha + \beta\sigma_{b,EMI}$.~~

As already discussed, the high correlation of the means and the standard deviations of the two series are central for this procedure to be of practical interest. In short, the procedure can be summarized as follows: (i) An area is monitored via EMI survey and a few TDR calibration measurements are collected concurrently. (ii) The availability of the two different datasets allows performing the regression ~~To explain this with an example, let us assume an experiment (like that described herein) has been carried out in a calibration field within the area to be monitored by an EMI sensor; the experiment would allow regressions to be built~~ for the mean and the standard deviation of the original EMI inversion results and the filtered TDR data, like those shown in ~~figures~~ Fig.s ~~6b~~ 8b and 9~~7~~b.~~.~~ (iv) These statistical parameters can be promptly used for the calculation of the coefficients α and β to be inserted into Eq. 10. (v) ~~Now let us take a set of ECa readings in the area to be monitored. After inversion, these ECa data provide a set of~~ ~~$\sigma_{b,EMI}$~~ ~~values. For the reasons discussed above,~~The original EMI inversion results ~~we know that these values do not represent the actual~~are not always reliable ~~values one~~ when compared with the direct ~~would~~ measurements ~~directly~~ obtained by using a TDR probe. Rather, they only contain the low-frequency information supplied by TDR (most likely, together with some shifts connected with the poor absolute calibration of the EMI system and/or the working conditions, e.g., the temperature). Thus, for quantitative analyses, it may be crucial to transform the original EMI result $\sigma_{b,EMI}$ into a new, calibrated section $\sigma^{rg}_{b,EMI}$ by means of the linear mapping in Eq. 10~~We now have a workflow to convert these~~ ~~$\sigma_{b,EMI}$~~ ~~data into the corresponding filtered TDR values~~.

~~In other words, t~~The proposed workflow enables us to translate the original non-calibrated $\sigma_{b,EMI}$ data into the actual σ_b we would collect in ideal conditions, and which would perfectly match "low-resolution" TRD measurements. ~~The workflow requires:~~

~~1. The mean and the standard deviation of EMI, which can be calculated by the $\sigma_{b,EMI}$ data;~~

~~2. The mean and the standard deviation of filtered TDR, which can be calculated by the regressions from the calibration experiment (as in figures 6b and 7b);~~

~~These statistics may now be used to evaluate coefficients α and β to be used in equation (18) to convert the original $\sigma_{b,EMI}$ data into as many $\sigma^{rg}_{b,TDR(FLT)}$ values. Hence, $\sigma^{rg}_{b,TDR(FLT)}$~~ $\sigma^{rg}_{b,EMI}$ is our best possible estimation of the true electrical conductivity at the scale of investigation of the EMI survey: it is the original $\sigma_{b,EMI}$ after the application of the appropriate rescaling and shifts deduced by the more reliable and absolutely calibrated TDR measurements.

Conclusions

The objective of the paper ~~was~~ is to infer the bulk electrical conductivity distribution in the root zone from multi-height (potentially non-calibrated) EMI readings. TDR direct measurements ~~were~~ are used as ground-truth σ_b data to evaluate the correctness of the σ_b estimations generated by EMI inversion. For all four transects and for all three depth-layers considered in this study, the $\sigma_{b,EMI}$ values underestimate the $\sigma_{b,TDR}$ measurements, such that the MRA line generally lies above the 1:1 line. Also, a considerable scatter around the MRA line was observed for all ~~four~~ transects.

The proposed analysis ~~allowed~~ allows ~~discussion~~ discussing ~~of~~ the physical reasons for the differences between EMI- and TDR-based electrical conductivity and developing an approach to calibrate the original $\sigma_{b,EMI}$ by using the $\sigma_{b,TDR}$ measurements. Our approach is based on the MRA coefficients and, hence, on the statistical parameters (mean and standard deviation) of the two series. Specifically, the approach looks for a systematic correction of the bias based on well-defined statistical sources of the discrepancies. A low-pass filtering has been carried out on the TDR data to obtain a significantly high correlation between the standard deviations of the two data series. After that, a simple linear transformation can be applied to the originally inverted EMI section $\sigma_{b,EMI}$ to get a calibrated σ_b result. ~~A significant high correlation was found for the means and the standard deviations of the two series, especially after filtering the TDR data. This is crucial for the practical application of our methodology.~~

The proposed strategy lies ~~in the fact~~on the assumption that ~~that~~ TDR direct measurements supply absolutely calibrated observations of the electrical conductivity of the soil and ~~hence~~ can be effectively used to calibrate the conductivity distributions inferred from EMI data. The availability of EMI calibrated data paves the way to reliable reconstructions of the electrical conductivity distribution over large areas (typical for EMI surveys, but not for TDR campaigns) unaffected by the usual EMI miscalibrations. This, in turn, can result in the possibility of effective time-lapse surveys and/or in consistent merging of subsequent surveys ~~(at any time the dynamic components of the system under investigation can be neglected)~~.

On the other hand, the proposed statistical workflow for making the TDR measurement comparable with the associated EMI results provides a more ~~more~~ sophisticated approach than simple smoothing to upscale the TDR data. Thus, from the opposite perspective, the approach in question can be used to tackle the problems connected with handling the TDR data characterized by excessively high spatial resolution.

~~Finally, the approach used here allows TDR calibration measurements to be used not necessarily at the same sites and in the same quantities as EMI readings, as it is based on means and standard deviations and does not require site-by-site data comparison.~~

References

Abdu, H., D.A. Robinson, and S.B. Jones. 2007. Comparing bulk soil electrical conductivity determination using the DUALEM-1S and EM38-DD electromagnetic induction instruments. *Soil Sci. Soc. Am. J.* 71 (1):189-196. doi: 10.2136/sssaj2005.0394.

Amezketa, E. 2006. An integrated methodology for assessing soil salinization, a pre-condition for land desertification. *J. Arid Environ.* 67 (4):594-606. doi: 10.1016/j.jaridenv.2006.03.010.

Beard, L. P, and J. E. Nyquist. 1998. Simultaneous inversion of airborne electromagnetic data for resistivity and magnetic permeability. Geophysics 63 (5): P1556-1564.

Bechtold, M., J.A. Huisman, L. Weihermüller, and H. Vereecken. 2010. Accurate determination of the bulk electrical conductivity with the TDR100 cable tester. *Soil Sci. Soc. Am. J.* 74, 495–501

Borchers, B., T. Uram, and J.M.H. Hendrickx. 1997. Tikhonov regularization of electrical conductivity depth profiles in field soils. *Soil Sci. Soc. Am. J.* 61 (4):1004-1009. doi: 10.2136/sssaj1997.03615995006100040002x.

Cassiani, G., N. Ursino, R. Deiana, G. Vignoli, J. Boaga, M. Rossi, M. T. Perri, M. Blaschek, R. Duttmann, S. Meyer, R. Ludwig, A. Saddu, P. Dietrich, and U. Werban. *Vadose Zone J.* doi:10.2136/vzj2011.0195

Coppola, A., G. Dragonetti, A. Comegna, N. Lamaddalena, B. Caushi, M.A. Haikal, and A. Basile. 2013. Measuring and modeling water content in stony soils. *Soil Till. Res*. 128:9-22.

Coppola, A., K. Smettem, A. Ajeel, A. Saeed, G. Dragonetti, A. Comegna, N. Lamaddalena, and A. Vacca. 2016. Calibration of an electromagnetic induction sensor with time-domain reflectometry data to monitor rootzone electrical conductivity under saline water irrigation. *Eur. J. of Soil Sci.* 67 (6):737-748. doi: 10.1111/ejss.12390.

Coppola, A., N. Chaali, G. Dragonetti, N. Lamaddalena, and A. Comegna. 2015. Root uptake under non-uniform root-zone salinity. *Ecohydrology*. 8 (7):1363-1379. doi: 10.1002/eco.1594.

Coppola, A., A. Comegna, G. Dragonetti, M. Dyck, A. Basile, N. Lamaddalena, M. Kassab, and V. Comegna. 2011. Solute transport scales in an unsaturated stony soil. *Adv. Water Resour*. 34 (6):747-759. doi: http://dx.doi.org/10.1016/j.advwatres.2011.03.006.

Corwin, D.L., and S.M. Lesch. 2005. Apparent soil electrical conductivity measurements in agriculture. *Comput. Electron. Agr.* 46 (1):11-43.

Cox, N.J. 2006. Assessing agreement of measurements and predictions in geomorphology. *Geomorphology*. 76 (3):332-346.

Dalton, F. N., W. N. Herkelrath, D. S. Rawlins, and J. D. Rhoades. 1984. Time domain reflectometry: Simultaneous measurement of soil water content and electrical conductivity with a single probe. *Science* 224, 989–990.

Deidda, G.P., E. Bonomi, and C. Manzi. 2003. Inversion of electrical conductivity data with Tikhonov regularization approach: some considerations. *Ann. Geophys*.

Deidda, G.P., C. Fenu, and G. Rodriguez. 2014. Regularized solution of a nonlinear problem in electromagnetic sounding *Inverse Probl*. 30 (12):125014.

Deidda, G.P., P. Diaz De Alba, and G. Rodriguez. 2017. Identifying the magnetic permeability in multi-frequency EM data inversion. *Submitted*.

Díaz de Alba, P., and G. Rodriguez. 2016. Regularized Inversion of Multi-Frequency EM Data in Geophysical Applications. In *Trends in Differential Equations and Applications*, 357-369. Springer.

Doolittle, J.A., and E.C. Brevik. 2014. The use of electromagnetic induction techniques in soils studies. *Geoderma* . 223:33-45.

Farquharson, C. G., Oldenburg, D. W., and Routh, P. S. 2003. Simultaneous 1D inversion of loop-loop electromagnetic data for both magnetic susceptibility and electrical conductivity. Geophysics. 68, 1857–1869.

Ferré, P.A., J. D. Redman, D.L. Rudolph, and R.G. Kachanoski. 1998a. The dependence of the electrical conductivity measured by time domain refiectometry on the water content of a sand. *Water Resour. Res*. 34 (5):1207-1213

Ferré~~re~~, P.A., J.H. Knight, D.L. Rudolph, and R.G. Kachanoski. 1998b. The sample areas of conventional and alternative time domain reflectometry probes. *Water Resour. Res*. 34 (11):2971-2979.

Fiandaca, G., J. Doetsch, G. Vignoli, and E. Auken. 2015. Generalized focusing of time-lapse changes with applications to direct current and time-domain induced polarization inversions. *Geophys. J. Int*. 203 (2):1101-1112. doi: 10.1093/gji/ggv350.

Freedman, D., R. Pisani, R. Purves, and A. Adhikari. 1991. Statistics (2nd ed.). New York: W. W. Norton.

Gebbers, R., E. Lück, M. Dabas, and H. Domsch. 2009. Comparison of instruments for geoelectrical soil mapping at the field scale. *Near Surf. Geophys*. 7 (3):179-190. doi: 10.3997/1873-0604.2009011

Günther, T. 2011. Timelapse ERT inversion approaches and their applications. *Geoelectric Monitoring*:91.

Heimovaara, T.J., A.G. Focke, W. Bouten, and J.M. Verstraten. 1995. Assessing temporal variations in soil water composition with time domain reflectometry. *Soil Sci. Soc. Am. J.* 59 (3):689-698. doi: 10.2136/sssaj1995.03615995005900030009x.

Hendrickx, J.M.H., B. Borchers, D.L. Corwin, S.M. Lesch, A.C. Hilgendorf, and J. Schlue. 2002. Inversion of soil conductivity profiles from electromagnetic induction measurements. *Soil Sci. Soc. Am. J.*. 66 (3):673-685. doi: 10.2136/sssaj2002.6730.

Huisman, J.A., C. P. Lin, L. Weihermüller, H. Vereecken. 2008. Accuracy of Bulk Electrical Conductivity Measurements with Time Domain Reflectometry. *Vadose Zone J.* 7, 426–433

Koestel, J., A. Kemna, M. Javaux, A. Binley, H. Vereecken. 2008. Quantitative imaging of solute transport in an unsaturated and undisturbed soil monolith with 3-D ERT and TDR. *Water Resour. Res.* 44, W12411, doi:10.1029/2007WR006755.

Lavoué, F., J. van der Kruk, J. Rings, F. André, D. Moghadas, J.A. Huisman, S. Lambot, L. Weihermüller, J. Vanderborght, and H. Vereecken. 2010. Electromagnetic induction calibration using apparent electrical conductivity modelling based on electrical resistivity tomography. *Near Surf. Geophys*. 8 (6):553-561.

Lesch, S.M., J.D. Rhoades, L.J. Lund, and D.L. Corwin. 1992. Mapping soil salinity using calibrated electromagnetic measurements. *Soil Sci. Soc. Am. J.*. 56 (2):540-548. doi: 10.2136/sssaj1992.03615995005600020031x.

Ley-Cooper, A.Y., A. Viezzoli, J. Guillemoteau, G. Vignoli, J. Macnae, L. Cox, and T. Munday. 2015. Airborne electromagnetic modelling options and their consequences in target definition. *Explor. Geophys*. 46 (1):74-84. doi: 10.1071/eg14045.

Lin, K. 1989. A concordance correlation coefficient to evaluate reproducibility. *Biometrics*:255-268.

Lin, C.P., C. C. Chung, J. A. Huisman, and S. H. Tang. 2008. Clarification and calibration of reflection coefficient for time domain reflectometry electrical conductivity measurement. *Soil Sci. Soc. Am. J.* 72, 1033-104072.

Lin, C.P., C. C. Chung, and S. H. Tang. 2007. Accurate time domain reflectometry measurement of electrical conductivity accounting for cable resistance and recording time. *Soil Sci. Soc. Am. J.* 71,1278–1287.

Mallants, D., M. Vanclooster, M. Meddahi, and J. Feyen. 1994. Estimating solute transport in undisturbed soil columns using time-domain reflectometry. *Journal Contam. Hydrol*. 17 (2):91-109. doi: 10.1016/0169-7722(94)90016-7.

McNeill, J.D. 1980. Electromagnetic terrain conductivity measurement at low induction numbers. Geonics Limited Ontario, Canada.

Mester, A., J. Van Der Kruk, E. Zimmermann, and H. Vereecken. 2011. Quantitative Two-Layer Conductivity Inversion of Multi-Configuration Electromagnetic Induction Measurements. *Vadose Zone J*. 10:1319-1330. doi: 10.2136/vzj2011.0035.

Minsley, B.J., B.D. Smith, R. Hammack, J.I. Sams, and G. Veloski. 2012. Calibration and filtering strategies for frequency domain electromagnetic data. *J. Appl. Geophys*. 80:56-66. doi: 10.1016/j.jappgeo.2012.01.008.

Moghadas, D., F. André, J.H. Bradford, J. van der Kruk, H. Vereecken, and S. Lambot. 2012. Electromagnetic induction antenna modelling using a linear system of complex antenna transfer functions. *Near Surf. Geophys*. 10 (3):237-247. doi: 10.3997/1873-0604.2012002

Noborio, K. 2001. Measurement of soil water content and electrical conductivity by time domain reflectometry: A review. *Comput. Electron. Agric.* 31:213–237.

Nüsch, A.K., P. Dietrich, U. Werban, T. Behrens, and N. Prakongkep. 2010. Acquisition and reliability of geophysical data in soil science. Paper read at 19th world congress of soil science, soil solutions for a changing world, Brisbane, Australia.

Oberdörster, C., J. Vanderborght, A. Kemna, and H. Vereecken. 2010. Investigating preferential flow processes in a forest soil using time domain reflectometry and electrical resistivity tomography. *Vadose Zone J*. 9 (2):350-361.

Pagliara, G., and G. Vignoli. 2006. Focusing inversion techniques applied to electrical resistance tomography in an experimental tank. In *XI International Congress of the International Association for Mathematical Geology*.

Rhoades, J.D., and D.L. Corwin. 1981. Determining soil electrical conductivity-depth relations using an inductive electromagnetic soil conductivity meter. *Soil Sci. Soc. Am. J.*. 45 (2):255-260.

Rhoades, J.D., and J. van Schilfgaarde. 1976. An electrical conductivity probe for determining soil salinity. *Soil Sci. Soc. Am. J.* 40 (5):647-651. doi: 10.2136/sssaj1976.03615995004000050016x.

Robinson, D.A., and S.P. Friedman. 2003. A method for measuring the solid particle permittivity or electrical conductivity of rocks, sediments, and granular materials. *J. Geophys. Res-Sol Ea*. 108 (B2):2076. doi: 10.1029/2001JB000691.

Robinson, D. A., S. B. Jones, J. M. Wraith, D. Or, and S. P., Friedman. 2003. A review of advances in dielectric and electrical conductivity measurement using time domain reflectometry. *Vadose Zone J.* 2, 444–475.

Robinson, D.A., I. Lebron, S.M. Lesch, and P. Shouse. 2004. Minimizing Drift in Electrical Conductivity Measurements in High Temperature Environments using the EM-38. *Soil Sci. Soc. Am. J.*. 68 (2):339-345. doi: 10.2136/sssaj2004.3390.

Robinson, D.A., H. Abdu, I. Lebron, and S.B. Jones. 2012. Imaging of hill-slope soil moisture wetting patterns in a semi-arid oak savanna catchment using time-lapse electromagnetic induction. *J. Hydrol*. 416–417:39-49. doi:https://doi.org/10.1016/j.jhydrol.2011.11.034.

Santos, F.A. Monteiro, J. Triantafilis, K.E. Bruzgulis, and J.A.E. Roe. 2010. Inversion of Multiconfiguration Electromagnetic (DUALEM-421) Profiling Data Using a One-Dimensional Laterally Constrained Algorithm. *Vadose Zone J*. 9:117-125. doi: 10.2136/vzj2009.0088.

Sheets, K.R., and J.M.H. Hendrickx. 1995. Noninvasive soil water content measurement using electromagnetic induction. *Water Resour. Res*. 31 (10):2401-2409.

Shumway, R.H. 1988. *Applied Time Series Analysis*: Prentice-Hall, Englewood Cliffs, NJ.

Sudduth, K.A., S.T. Drummond, and N.R. Kitchen. 2001. Accuracy issues in electromagnetic induction sensing of soil electrical conductivity for precision agriculture. *Comput. Electron. Agr*. 31 (3):239-264. doi: 10.1016/S0168-1699(00)00185-X.

Thomsen, A., K. Schelde, P. Drøscher, F. Steffensen. 2007. Mobile TDR for geo-referenced measurement of soil water content and electrical conductivity. *Precision Agriculture* 8, 213–223

Topp, G. C., M. Yanuka, W. D. Zebchuk, and S. Zegelin. 1988. Determination of electrical conductivity using time domain Reflectometry: Soil and water experiments in coaxial lines. *Water Resour. Res.* 24, 945–952.

Triantafilis, J., G.M. Laslett, and A.B. McBratney. 2000. Calibrating an electromagnetic induction instrument to measure salinity in soil under irrigated cotton. *Soil Sci. Soc. Am. J*. 64 (3):1009-1017. doi: 10.2136/sssaj2000.6431009x.

Ursino, N., G. Cassiani, R. Deiana, G. Vignoli and J. Boaga. 2014. Measuring and modeling water-related soil–vegetation feedbacks in a fallow plot. *Hydrol. Earth Syst. Sci.* 18, 1105–1118.

Vignoli, G., G. Fiandaca, A.V. Christiansen, C. Kirkegaard, and E. Auken. 2015. Sharp spatially constrained inversion with applications to transient electromagnetic data. *Geophys. Prospect*. 63 (1):243-255.

Vignoli, G., V. Sapia, A. Menghini, and A. Viezzoli. 2017. Examples of Improved Inversion of Different Airborne Electromagnetic Datasets Via Sharp Regularization. *J. Environ. Eng. Geophys.* 22 (1):51-61. doi: 10.2113/jeeg22.1.51.

Vignoli, G., R. Deiana, and G. Cassiani. 2012. Focused inversion of vertical radar profile (VRP) traveltime data. *Geophysics*. 77 (1):H9-H18. doi: 10.1190/geo2011-0147.1.

V~~v~~on Hebel, C., S. Rudolph, A.Mester, J.A. Huisman, P. Kumbhar, H. Vereecken, and J. van der Kruk. 2014. Three-dimensional imaging of subsurface structural patterns using quantitative large-scale multiconfiguration electromagnetic induction data. *Water Resour. Res*. 50 (3):2732-2748.

Wait, J.R. 1982. Geo-Electromagnetism. In *Geo-Electromagnetism*, 1-67. Academic Press.

Ward, S.H., and G.W. Hohmann. 1988. Electromagnetic theory for geophysical applications. *Electromagnetic methods in applied geophysics.*

Weerts A. H., J. A. Huisman, and W. Bouten, .2001. Information content of time domain reflectometry waveforms. *Water Resources Research.* 37 (5), 1291–1299

Wraith, J.M., B.L. Woodbury, W.P. Inskeep, and S.D. Comfort. 1993. A simplified waveform analysis approach for monitoring solute transport using time-domain reflectometry. *Soil Sci. Soc. Am. J*. 57 (3):637-642.

Yao, R., and Jingsong Y. 2010. Quantitative evaluation of soil salinity and its spatial distribution using electromagnetic induction method. *Agr. Water Manage*. 97 (12):1961-1970. doi: 10.1016/j.agwat.2010.02.001.

Yu, M., and D.E. Dougherty. 2000. Modified total variation methods for three-dimensional electrical resistance tomography inverse problems. *Water Resour. Res*. 36 (7):1653-1664.

Zhdanov, M.S., G. Vignoli, and T. Ueda. 2006. Sharp boundary inversion in crosswell travel-time tomography. *J. Geophys. Eng*. 3 (2):122.

Zhdanov, M.S. 2002. Geophysical Inverse Theory and Regularization Problems Methods. ~~in Geochemistry and Geophysics, edited by S. Zhdanov Michael, xix-xxiii.~~ Elsevier.

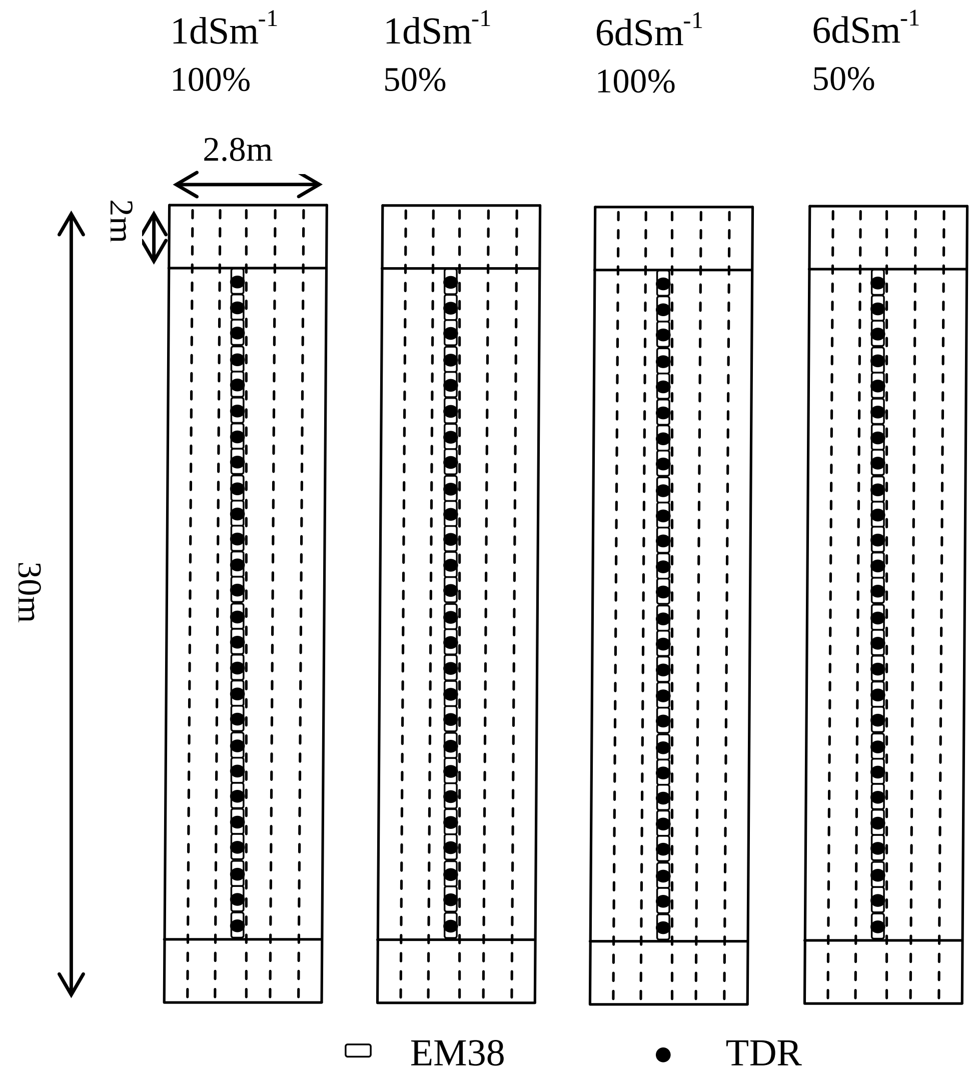

Figure 1. Schematic view of the experimental field

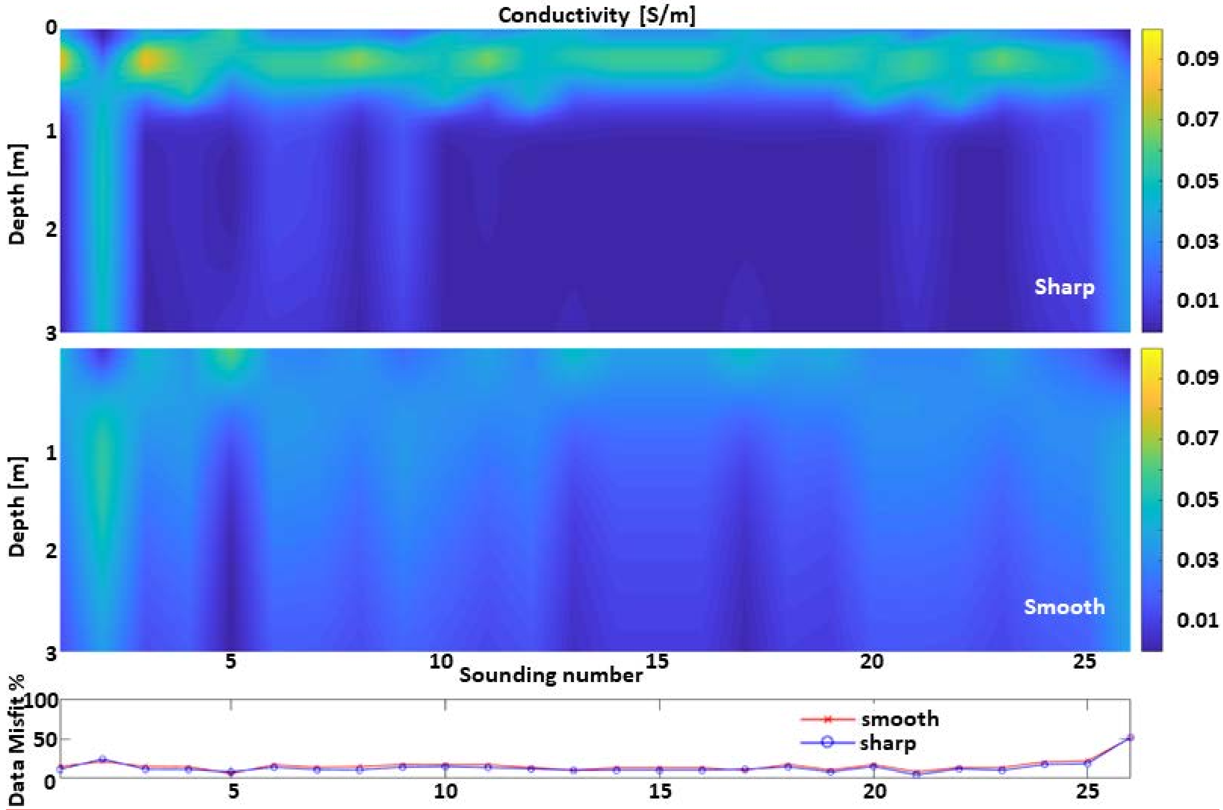

Conductivity [S/m]
Depth [m]
Sharp
Smooth
0.09
0.07
0.05
0.03
0.01
Sounding number
Data Misfit %
smooth
sharp

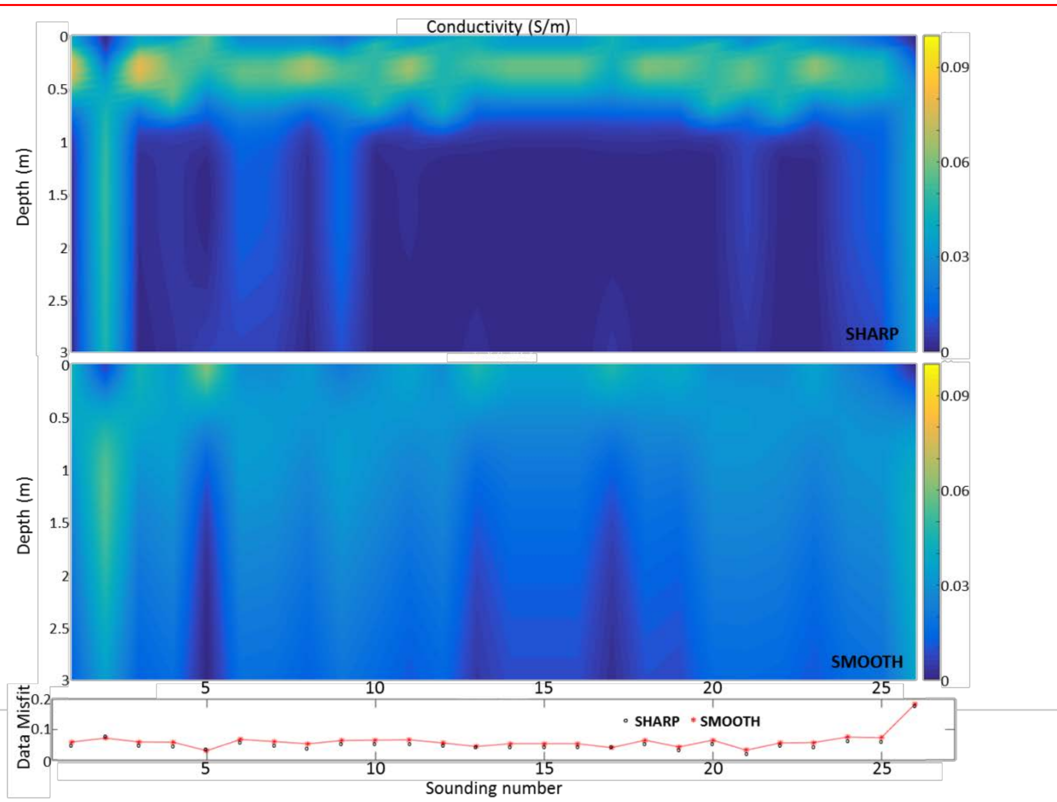

Conductivity (S/m)
Depth (m)
SHARP
SMOOTH
0.09
0.06
0.03
Data Misfit
SHARP
SMOOTH
Sounding number

Figure 2. Examples of sharp and smooth inversions applied to the ~~same~~ dataset 100-6dS. The results are shown together with their corresponding data misfit.

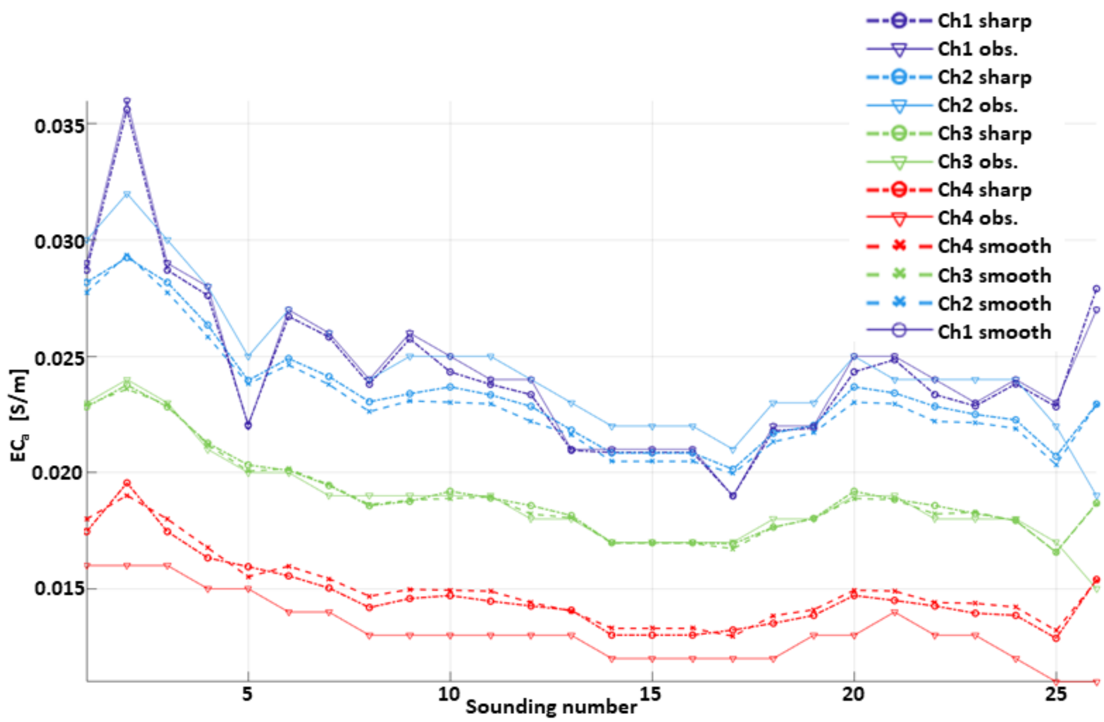

Figure 3. Comparison of the data fitting associated with the sharp and smooth inversions applied to the dataset 100-6dS (Fig. 2). The calculated data corresponding to the sharp and smooth results are shown together with the observations for each of the four measured channels (heights).

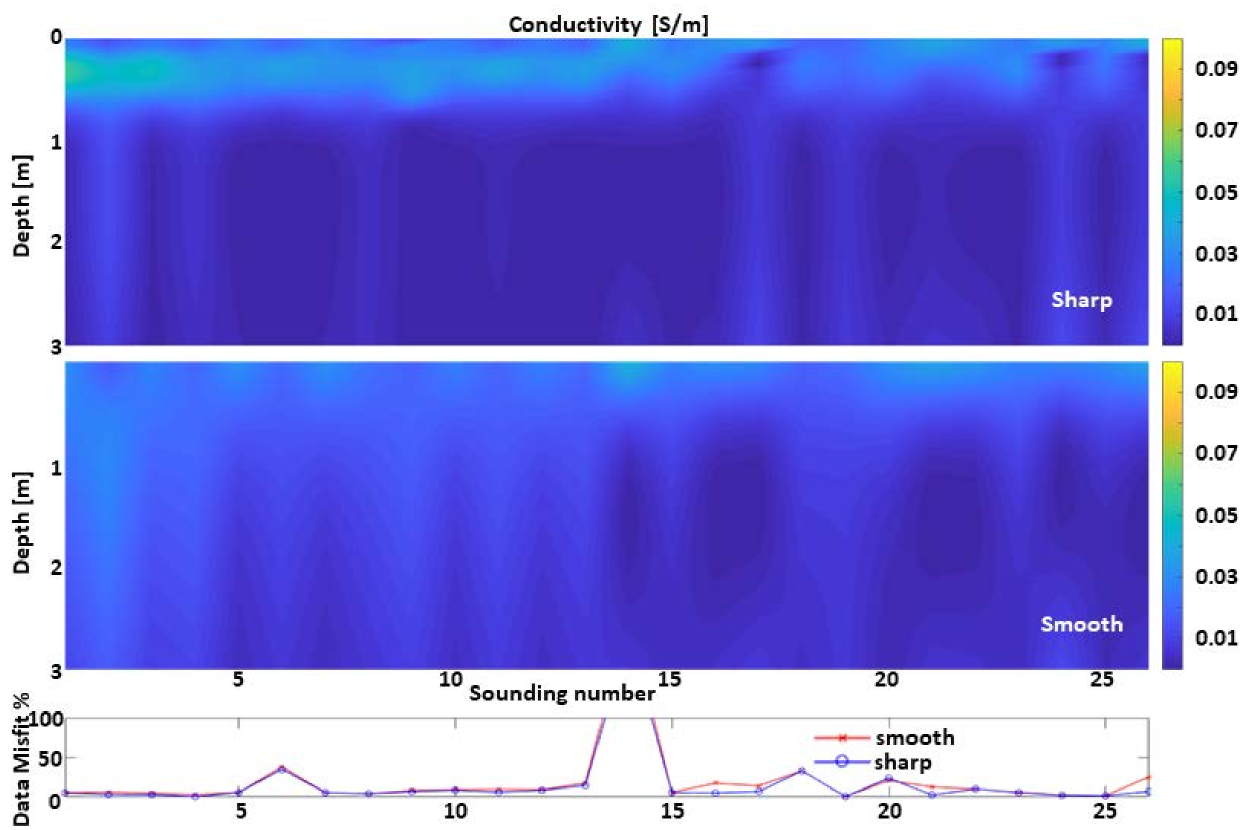

Figure 4. Examples of sharp and smooth inversions applied to the dataset 50-6dS. The results are shown together with their corresponding data misfit.

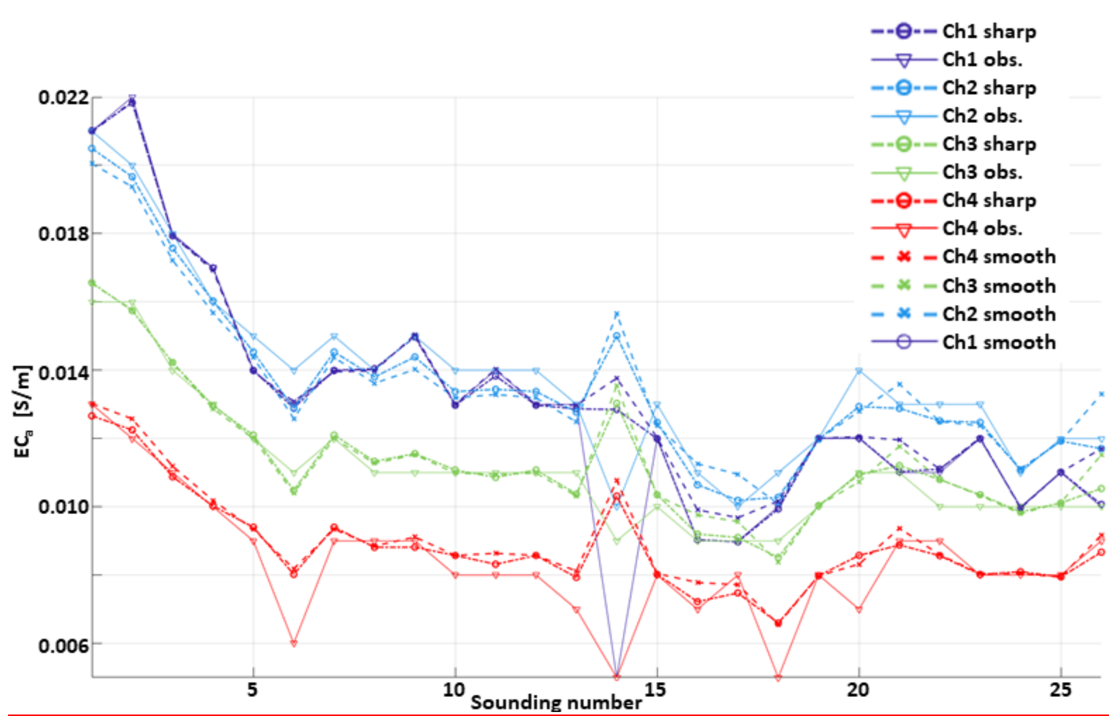

Figure 5. Comparison of the data fitting associated with the sharp and smooth inversions applied to the dataset 50-6dS (Fig. 4). The calculated data corresponding to the sharp and smooth results are shown together with the observations for each of the four measured channels (heights).

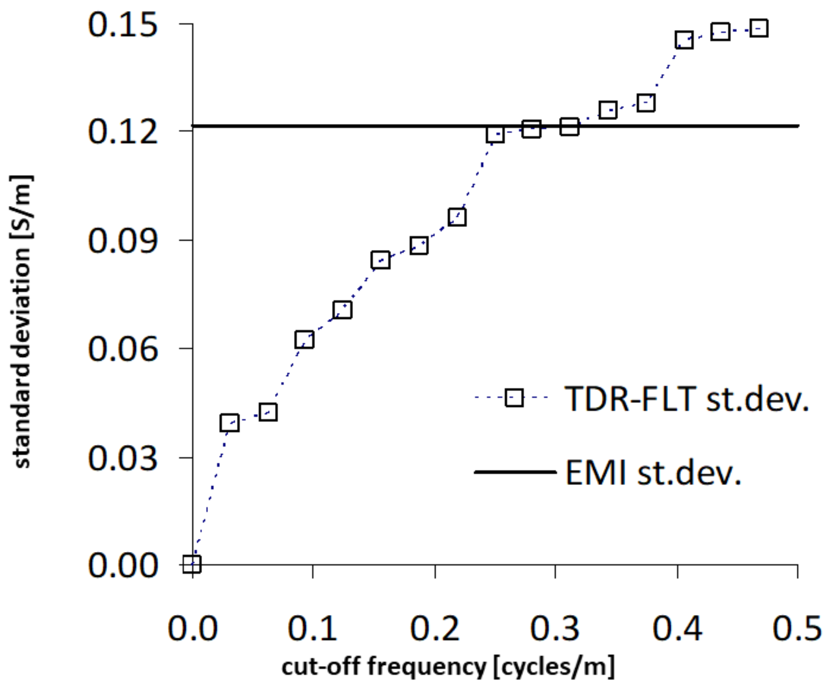
0.15
0.12
0.09
0.06
0.03
0.00
standard deviation [S/m]
0.0
0.1
0.2
0.3
0.4
0.5
cut-off frequency [cycles/m]
TDR-FLT st.dev.
EMI st.dev.

a

b

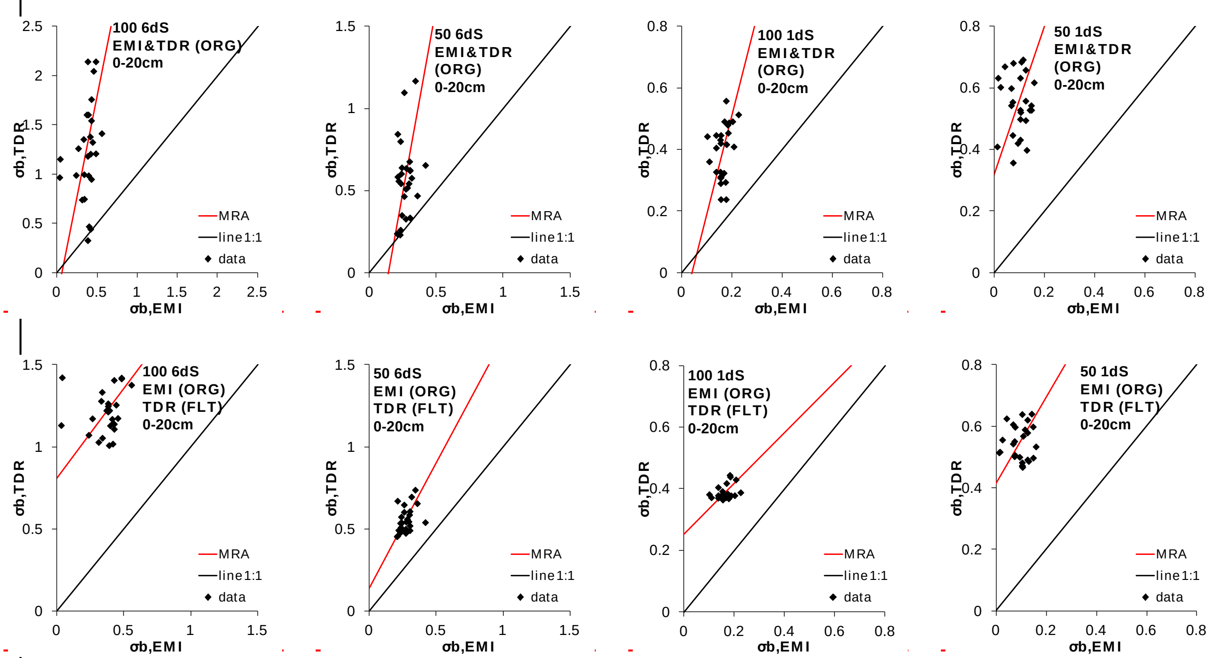
100 6dS
EMI&TDR (ORG)
0-20cm
50 6dS
EMI&TDR
(ORG)
0-20cm
100 1dS
EMI&TDR
(ORG)
0-20cm
50 1dS
EMI&TDR
(ORG)
0-20cm
100 6dS
EMI (ORG)
TDR (FLT)
0-20cm
50 6dS
EMI (ORG)
TDR (FLT)
0-20cm
100 1dS
EMI (ORG)
TDR (FLT)
0-20cm
50 1dS
EMI (ORG)
TDR (FLT)
0-20cm
σb,TDR
σb,EMI
MRA
line1:1
data

c

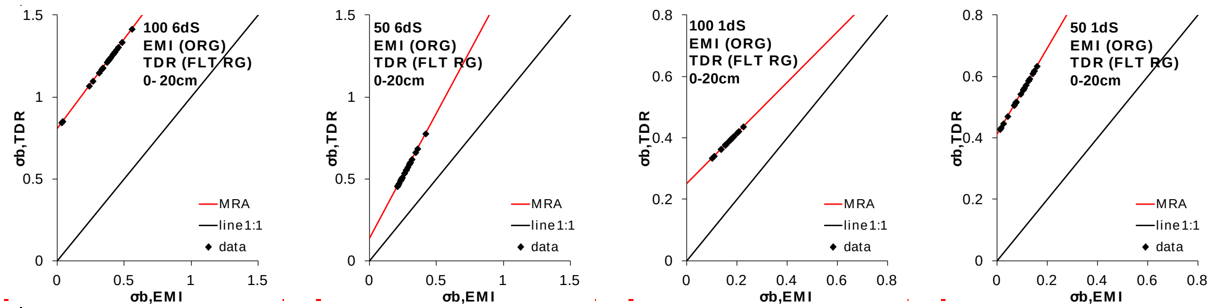

Figure ~~3~~6. Standard deviation of the EMI series (horizontal black line) for the 50-6dS transect at 0.2-0.4 m depth. The squares show the corresponding standard deviations for the TDR series for different level of filtering. The intersection of the EMI line with the TDR curve allows identifying the optimal cut-off frequency range (~0.313 cycles/m) to make the two standard deviations similar.~~Comparison between~~ ~~$\sigma_{b,TDR}$~~ ~~and~~ ~~$\sigma_{b,EMI}$~~ ~~for all four transects for the depth layer 0-20 cm. The graphs in the horizontal panels are respectively for: (a) Original EMI and TDR data; (b) original EMI and filtered TDR data (c) original EMI and filtered TDR data after regression (RG) based on MRA parameters~~

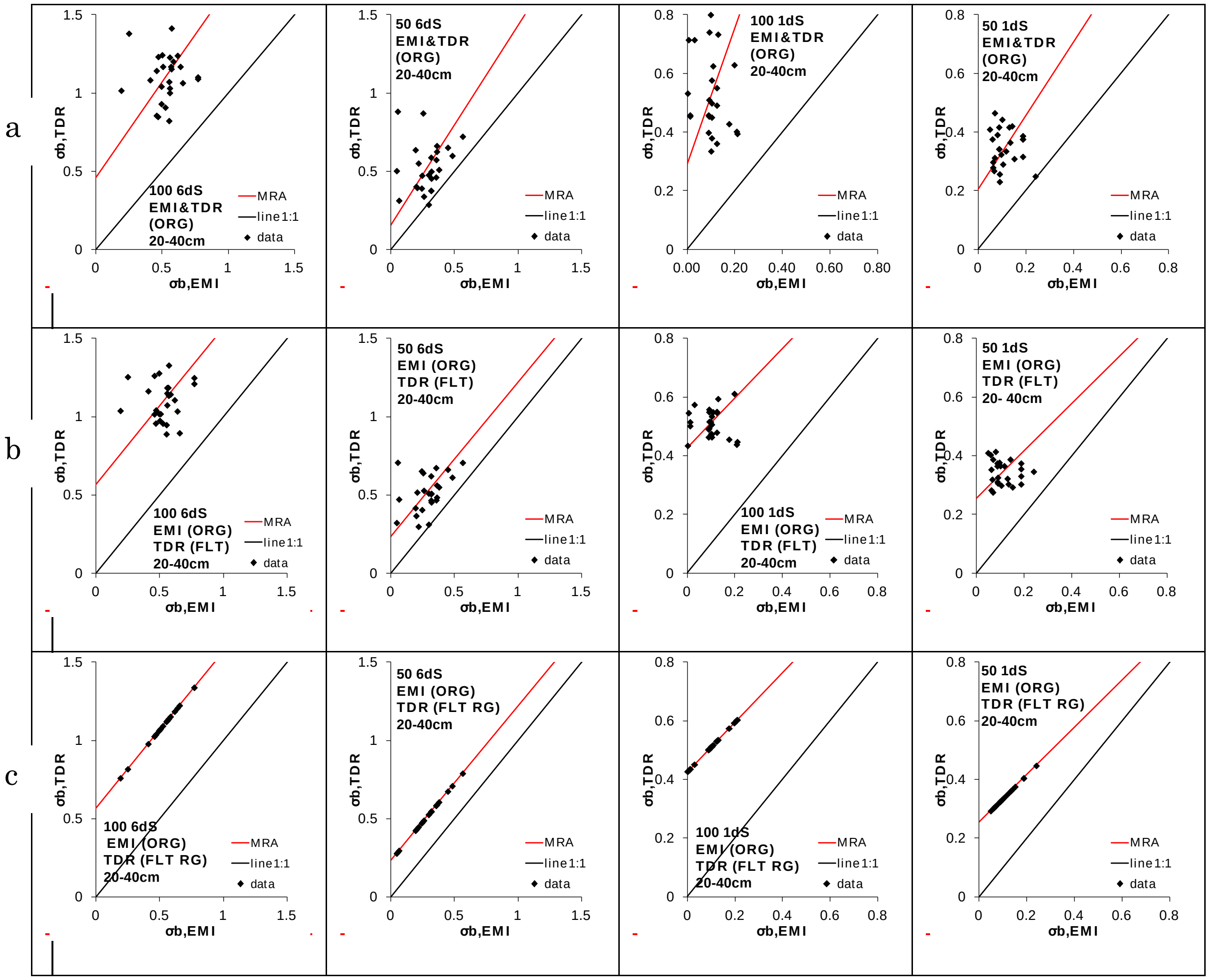
a
b
c
100 6dS
EMI&TDR
(ORG)
20-40cm
50 6dS
EMI&TDR
(ORG)
20-40cm
100 1dS
EMI&TDR
(ORG)
20-40cm
50 1dS
EMI&TDR
(ORG)
20-40cm
100 6dS
EMI (ORG)
TDR (FLT)
20-40cm
50 6dS
EMI (ORG)
TDR (FLT)
20-40cm
100 1dS
EMI (ORG)
TDR (FLT)
20-40cm
50 1dS
EMI (ORG)
TDR (FLT)
20- 40cm
100 6dS
EMI (ORG)
TDR (FLT RG)
20-40cm
50 6dS
EMI (ORG)
TDR (FLT RG)
20-40cm
100 1dS
EMI (ORG)
TDR (FLT RG)
20-40cm
50 1dS
EMI (ORG)
TDR (FLT RG)
20-40cm
MRA
line1:1
data
σb,TDR
σb,EMI
0
0.5
1
1.5
0.00
0.20
0.40
0.60
0.80
0.2
0.4
0.6
0.8

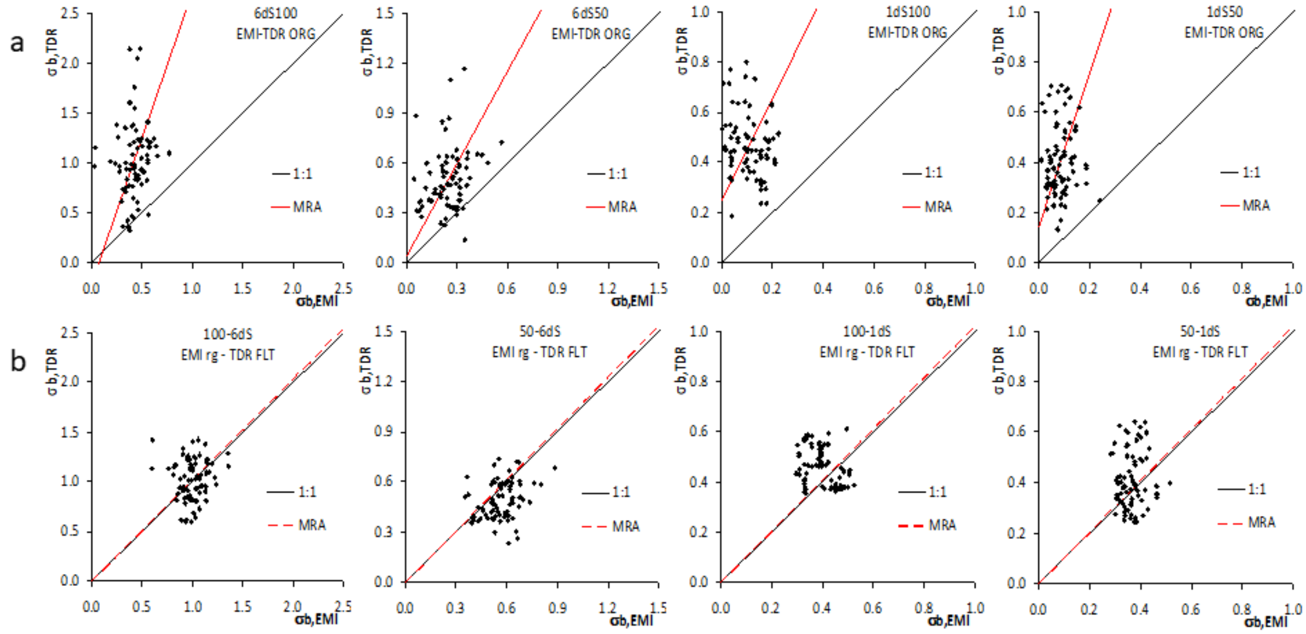

Figure 47. Comparison between $\sigma_{b,TDR}$ and $\sigma_{b,EMI}$ for all four transects for the depth range 0.0-0.6 m. The graphs in the top panels (a) show the original TDR and EMI data, while those in the bottom panels (b) the Filtered (FLT) TDR and EMI data after the regression based on MRA parameters (rg).~~Comparison between $\sigma_{b,TDR}$ and $\sigma_{b,EMI}$ for all four transects for the depth layer 20-40 cm. The graphs in the horizontal panels are respectively for: (a) Original EMI and TDR data; (b) original EMI and filtered TDR data (c) original EMI and filtered TDR data after regression (RG) based on MRA parameters~~

a

b

c

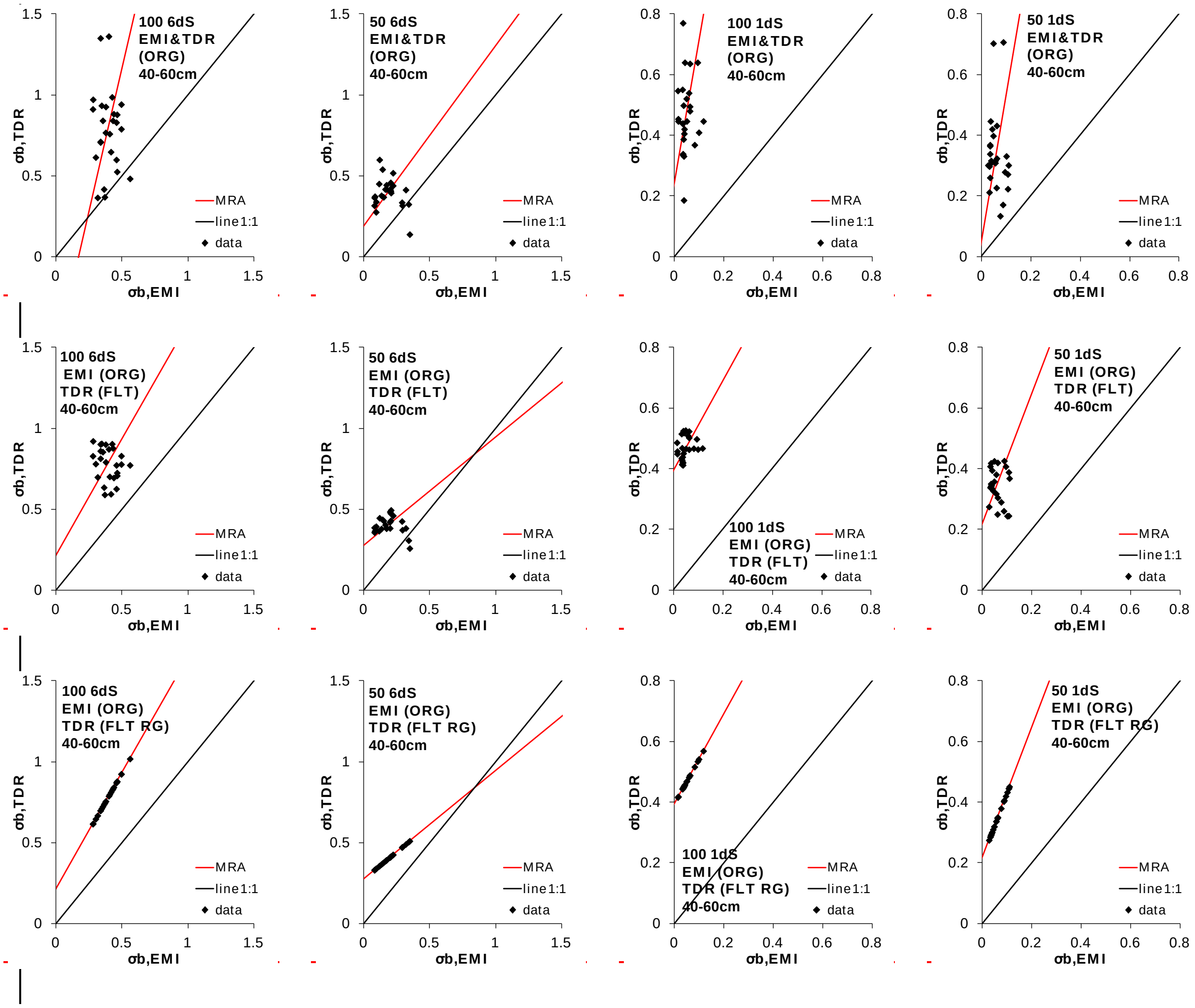

100 6dS
EMI&TDR
(ORG)
40-60cm
50 6dS
EMI&TDR
(ORG)
40-60cm
100 1dS
EMI&TDR
(ORG)
40-60cm
50 1dS
EMI&TDR
(ORG)
40-60cm
100 6dS
EMI (ORG)
TDR (FLT)
40-60cm
50 6dS
EMI (ORG)
TDR (FLT)
40-60cm
100 1dS
EMI (ORG)
TDR (FLT)
40-60cm
50 1dS
EMI (ORG)
TDR (FLT)
40-60cm
100 6dS
EMI (ORG)
TDR (FLT RG)
40-60cm
50 6dS
EMI (ORG)
TDR (FLT RG)
40-60cm
100 1dS
EMI (ORG)
TDR (FLT RG)
40-60cm
50 1dS
EMI (ORG)
TDR (FLT RG)
40-60cm
MRA
line1:1
data
σb,TDR
σb,EMI

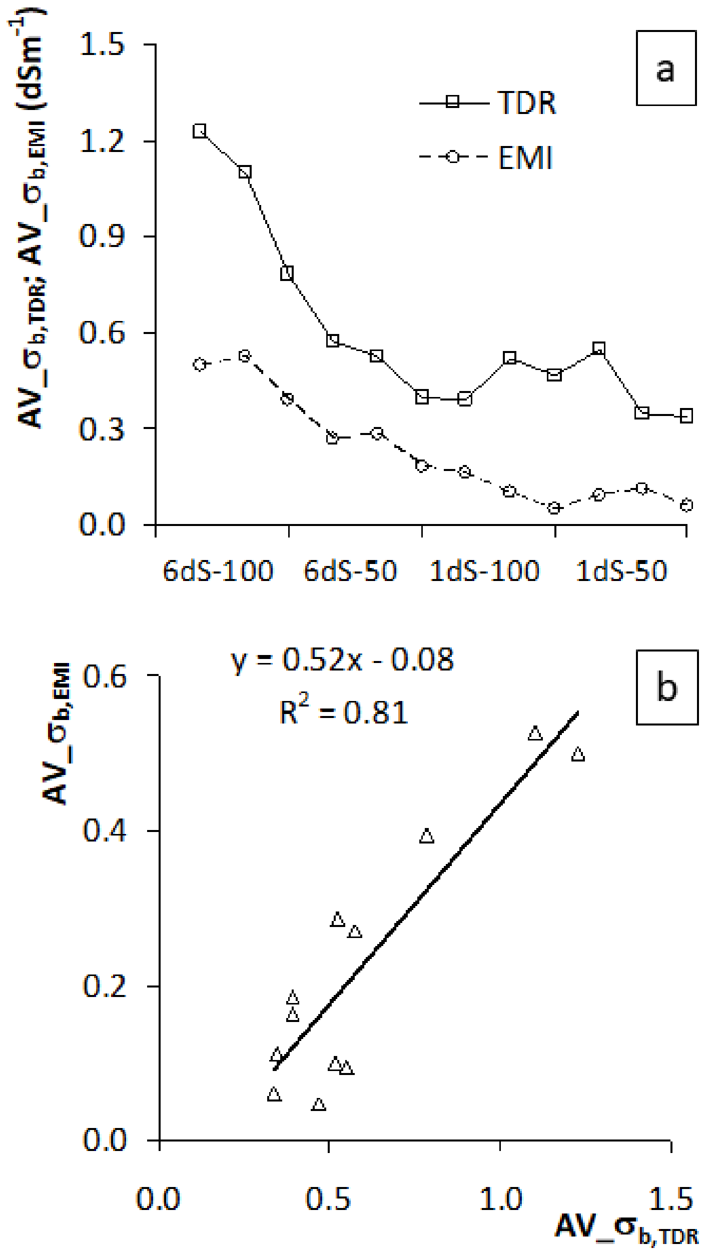

Figure 8~~5~~. (a) Comparison of the means for the two original series (squares-solid line for TDR, dcircles-dashed line for EMI); (b) The same comparison on a 1:1 plot (triangles-solid regression line). In the panel (a), the four cases are shown in sequence. For each case, the three values are for the three depth intervals 0.0-0.2, 0.2-0.4, and 0.4-0.6 m.~~Comparison between $\sigma_{b,TDR}$ and $\sigma_{b,EMI}$ for all four transects for the depth layer 40-60 cm. The graphs in the horizontal panels are~~

~~respectively for: (a) Original EMI and TDR data; (b) original EMI and filtered TDR data (c) original EMI and filtered TDR data after regression (RG) based on MRA parameters~~

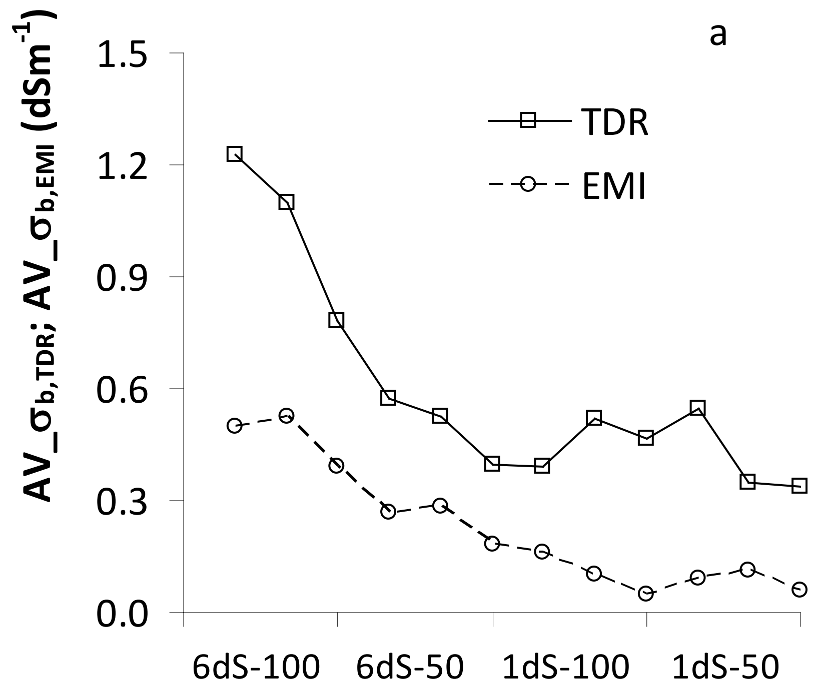
a
TDR
EMI
AV_σb,TDR; AV_σb,EMI (dSm-1)
1.5
1.2
0.9
0.6
0.3
0.0
6dS-100
6dS-50
1dS-100
1dS-50

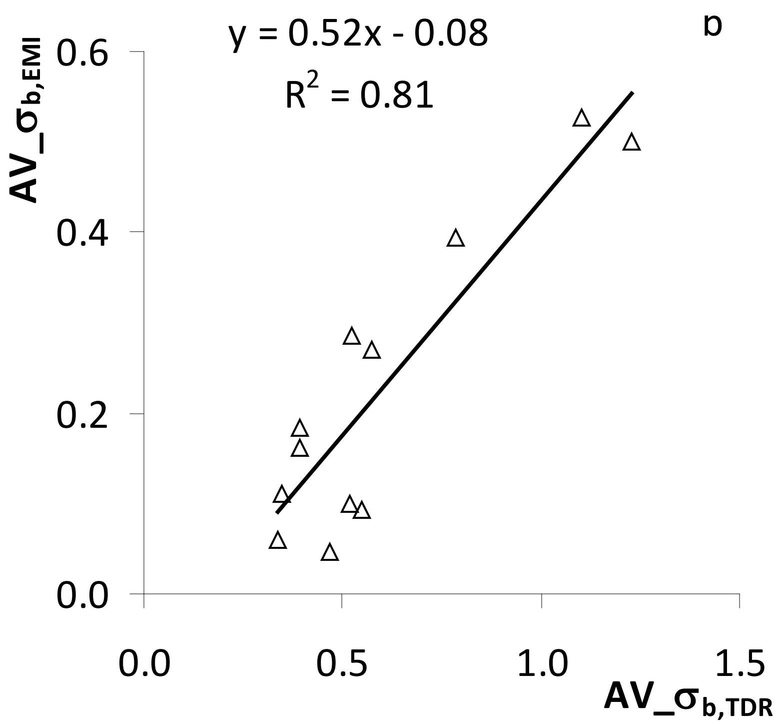
b
y = 0.52x - 0.08
R2 = 0.81
AV_σb,EMI
0.6
0.4
0.2
0.0
0.0
0.5
1.0
1.5
AV_σb,TDR

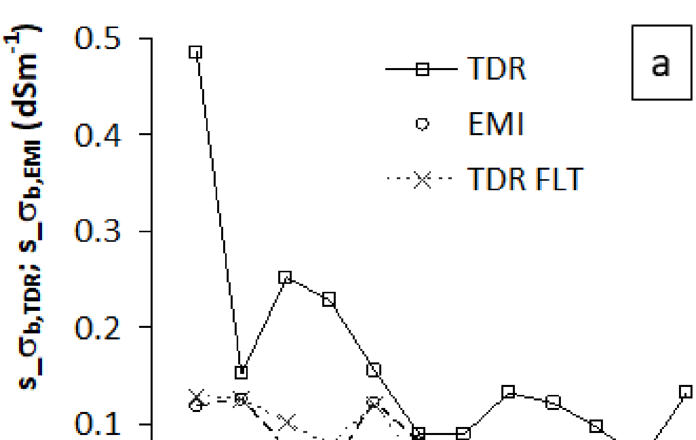
a
TDR
EMI
TDR FLT
s_σb,TDR; s_σb,EMI (dSm-1)
0.5
0.4
0.3
0.2
0.1

Figure ~~6~~9. (a) Comparison of the standard deviations of the TDR original series (squares-solid line), of the EMI original series (circles-dashed line), and of the filtered (FLT) TDR series (crosses-dashed line); (b) The same comparison on a 1:1 plot: the original TDR and EMI data (triangles-solid regression line); filtered (FLT) TDR and original EMI data (squares-dashed regression line). In the panel (a), the four cases are shown in sequence. For each case, the three values are for the three depth intervals 0.0-0.2, 0.2-0.4, and 0.4-0.6 m.

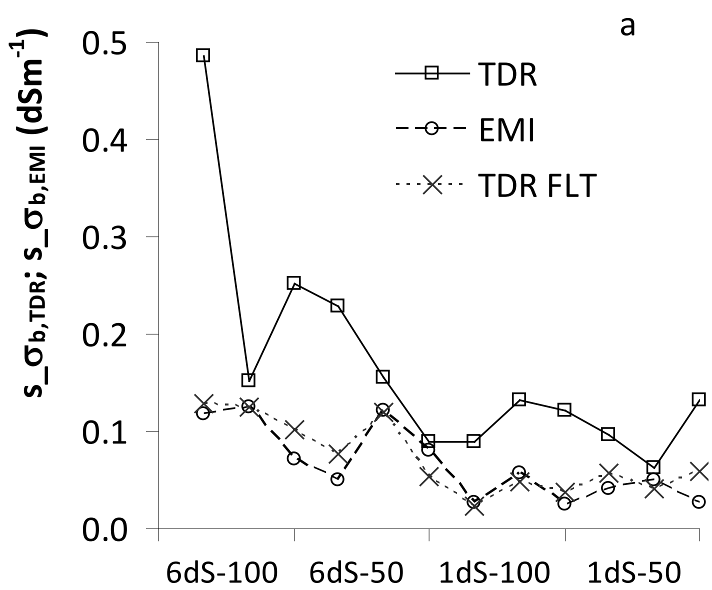

~~(a) Comparison of the means for the two original series (open squares-solid line for TDR, open circles-dashed line for EMI); (b) The same comparison on a 1:1 plot (open triangles-solid regression line). In figure 6a the four treatments are shown in sequence. For each treatment, the three values are for the three depths (0-20, 20-40 and 40-60 cm)~~

~~Figure 7. (a) Comparison of the standard deviations of the TDR original series (open squares-~~

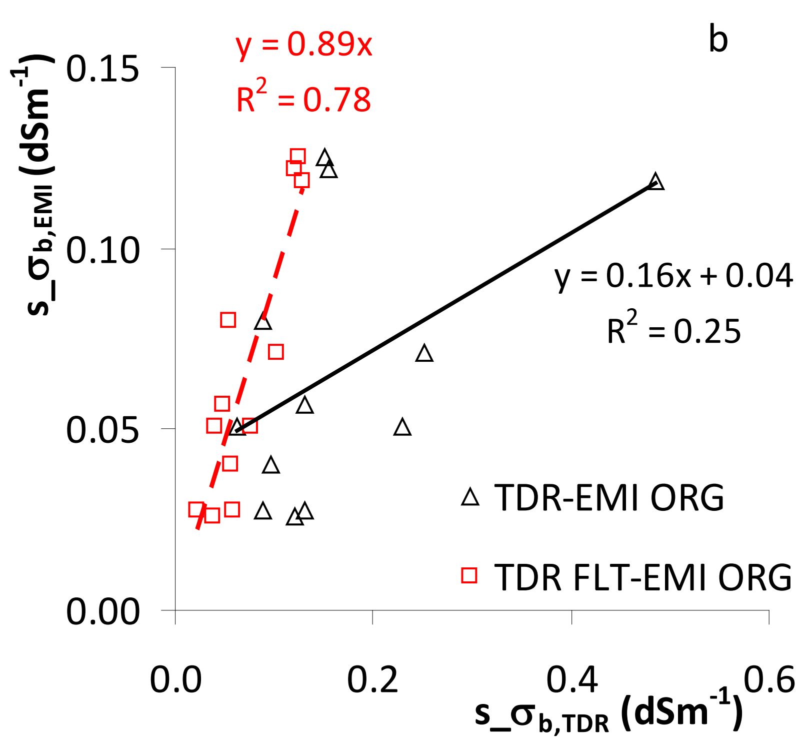

~~solid line), of the EMI original series (open circles-dashed line) and of the filtered TDR series (crosses-dashed line); (b) The same comparison on a 1:1 plot: original TDR and EMI data (open triangles-solid regression line); filtered TDR and original EMI data (open squares-dashed regression line). In figure 7a the four treatments are shown in sequence. For each treatment, the three values are for the three depths (0-20, 20-40 and 40-60 cm)~~

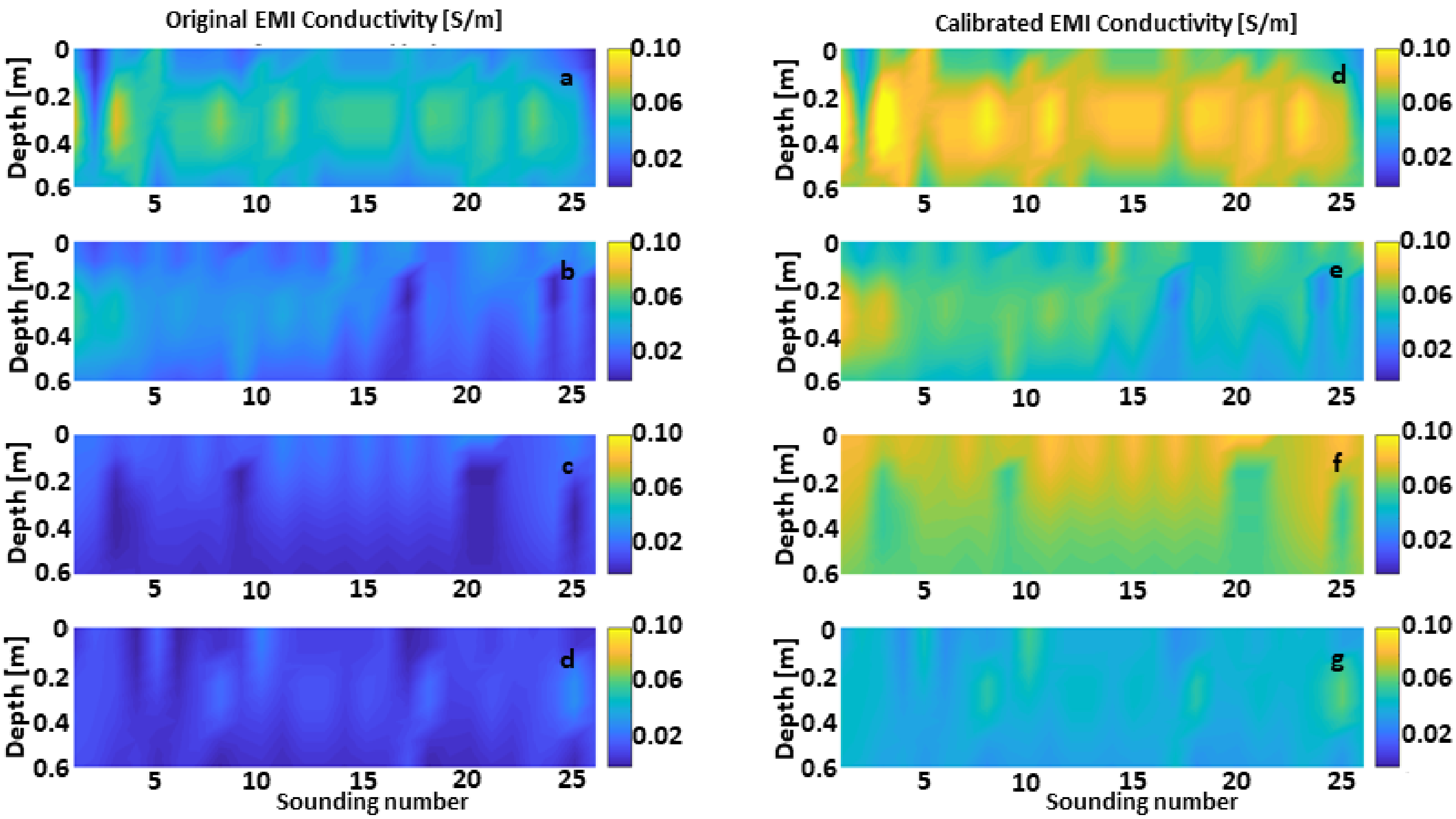
Original EMI Conductivity [S/m]
Calibrated EMI Conductivity [S/m]
Depth [m]
Sounding number
a
b
c
d
e
f
g
0.10
0.06
0.02

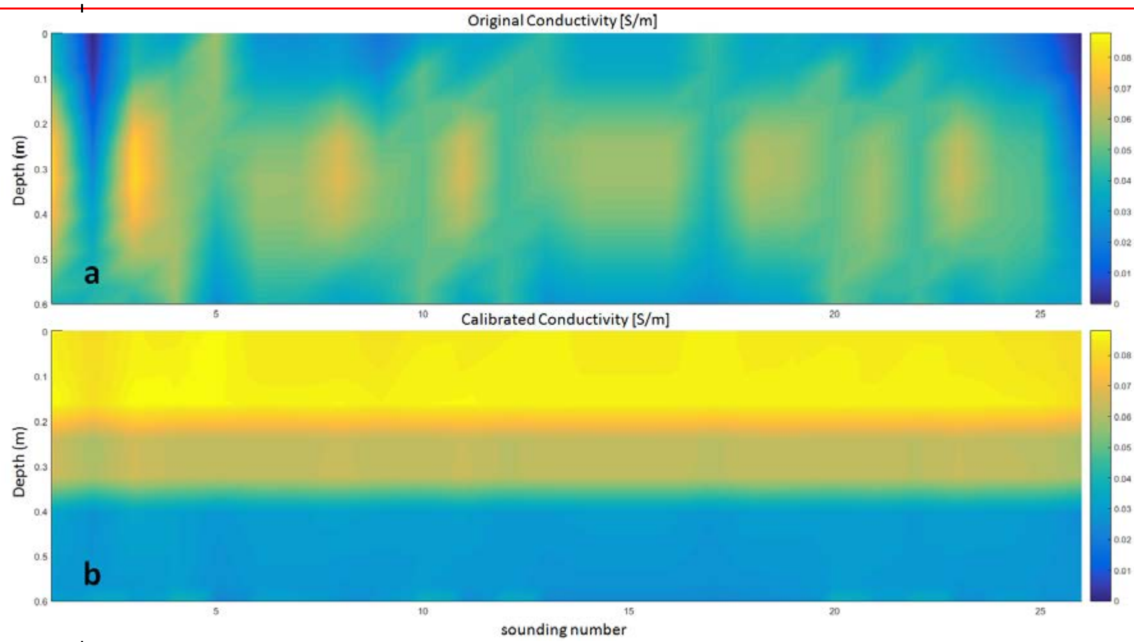
Original Conductivity [S/m]
Calibrated Conductivity [S/m]
Depth (m)
sounding number
a
b

Figure ~~8~~10. Maps of bulk electrical conductivity for the: (a) 100-6dS, (b) 50-6dS, (c) 100-1dS, (d) 50-1dS transects ~~obtained respectively by plotting the~~ showing the o~~o~~riginal $\sigma_{b,EMI}$ ~~(a) coming~~resulting from the ~~from the~~ inversion of the observed EMI ~~signal~~ data. Panels (d) to (g)~~and~~ show instead the corresponding results after the calibration via the TDR measurements (i.e., by applying Eq. 10).~~the calibrated~~ $\cancel{\sigma^{rg}_{b,TDR(FLT)}}$ ~~(b) obtained by applying the equation 18 to the~~ $\cancel{\sigma_{b,EMI}}$ ~~data of the first map~~

~~Table 1. Concordance parameters for the four transects for the TDR_ORG and EMI_ORG data. The table reports the Concordance, ρL, and the Pearson, ρP, correlation, as well as parameters α and β of the MRA line. The bias factor, Cb, is also shown.~~

Transect	C_b ~~Cb~~	ρ_L ~~ρL~~	ρ_P ~~ρP~~	β ~~β~~	α ~~α~~
100-1dS	0.10	0.02	0.33	2.04	0.25
50-1dS	0.10	0.00	0.08	3.06	0.14
100-6dS	0.18	0.02	0.07	2.92	-0.21
50-6dS	0.34	0.08	0.32	1.84	0.04

Table 1. Concordance parameters for the four transects for the TDR_ORG and EMI_ORG data. The table reports the Concordance, ρL, and the Pearson, ρP, correlation, as well as parameters α and β of the MRA line. The bias factor, Cb, is also shown.

Transect	C_b	ρ_L	ρ_P	β	α
100-1dS	0.74	0.24	0.33	1.02	0.29
50-1dS	0.62	0.05	0.08	1.02	0.27
100-6dS	0.87	0.06	0.07	1.02	0.57
50-6dS	0.79	0.25	0.32	1.02	0.31

~~Table 2. Concordance parameters for the four transects for the TDR_FLT and EMI_ORG data. The table reports the Concordance, ρL, and the Pearson, ρP, correlation, as well as parameters α and β of the MRA line. The bias factor, Cb, is also shown.~~

~~Transect~~	~~C_b~~	~~ρ_L~~	~~ρ_P~~	~~β~~	~~α~~
~~100-1dS~~	~~0.74~~	~~0.24~~	~~0.33~~	~~1.02~~	~~0.29~~
~~50-1dS~~	~~0.62~~	~~0.05~~	~~0.08~~	~~1.02~~	~~0.27~~
~~100-6dS~~	~~0.87~~	~~0.06~~	~~0.07~~	~~1.02~~	~~0.57~~
~~50-6dS~~	~~0.79~~	~~0.25~~	~~0.32~~	~~1.02~~	~~0.31~~

Table 2. Concordance parameters for the four transects for the TDR_FLT and EMI_ORG data. The table reports the Concordance, ρL, and the Pearson, ρP, correlation, as well as parameters α and β of the MRA line. The bias factor, Cb, is also shown.

~~Table 1. Concordance parameters for the four transects at depth 0-20 cm. The table reports the Concordance, ρ_L, and the Pearson, ρ_P, correlation, as well as parameters α and β of the MRA line. The bias factor, C_b, is also shown.~~

~~Graph panel~~	~~C_b 20cm~~	~~ρ_L 20cm~~	~~ρ_P 20cm~~	~~β 20cm~~	~~α 20cm~~
~~1dS-100~~					

~~**a**~~	~~0.08~~	~~0.02~~	~~0.31~~	~~3.20~~	~~-0.13~~
~~**b**~~	~~0.02~~	~~0.01~~	~~0.35~~	~~0.82~~	~~0.25~~
~~**c**~~	~~0.02~~	~~0.02~~	~~0.96~~	~~0.82~~	~~0.25~~
~~**1dS-50**~~					
~~**a**~~	~~0.04~~	~~0.0002~~	~~-0.01~~	~~2.39~~	~~0.32~~
~~**b**~~	~~0.02~~	~~0.0006~~	~~0.03~~	~~1.40~~	~~0.41~~
~~**c**~~	~~0.02~~	~~0.02~~	~~0.96~~	~~1.4~~	~~0.41~~
~~**6dS-100**~~					
~~**a**~~	~~0.12~~	~~0.03~~	~~0.25~~	~~4.10~~	~~-0.27~~
~~**b**~~	~~0.04~~	~~0.005~~	~~0.12~~	~~1.09~~	~~0.81~~
~~**c**~~	~~0.04~~	~~0.04~~	~~0.96~~	~~1.09~~	~~0.81~~
~~**6dS-50**~~					
~~**a**~~	~~0.16~~	~~0.03~~	~~0.22~~	~~4.52~~	~~-0.65~~
~~**b**~~	~~0.09~~	~~0.04~~	~~0.42~~	~~1.52~~	~~0.14~~
~~**c**~~	~~0.09~~	~~0.08~~	~~0.96~~	~~1.52~~	~~0.14~~

~~Table 2. Concordance parameters for the four transects at depth 20-40 cm. The table reports the Concordance, ρ_L, and the Pearson, ρ_P, correlation, as well as parameters α and β of the MRA line. The bias factor, C_b, is also shown.~~

~~Graph panel~~	~~C_b 40cm~~	~~ρ_L 40cm~~	~~ρ_P 40cm~~	~~β 40cm~~	~~α 40cm~~
~~1dS-100~~					
~~a~~	~~0.08~~	~~-0.02~~	~~-0.21~~	~~2.32~~	~~0.29~~
~~b~~	~~0.03~~	~~-0.002~~	~~-0.07~~	~~0.84~~	~~0.43~~
~~c~~	~~0.03~~	~~0.03~~	~~0.96~~	~~0.84~~	~~0.43~~
~~1dS-50~~					
~~a~~	~~0.10~~	~~-0.004~~	~~-0.04~~	~~1.25~~	~~0.21~~
~~b~~	~~0.07~~	~~-0.01~~	~~-0.13~~	~~0.81~~	~~0.25~~
~~c~~	~~0.07~~	~~0.07~~	~~0.96~~	~~0.81~~	~~0.25~~
~~6dS-100~~					
~~a~~	~~0.10~~	~~0.001~~	~~0.01~~	~~1.21~~	~~0.46~~
~~b~~	~~0.09~~	~~0.004~~	~~0.05~~	~~0.99~~	~~0.57~~
~~c~~	~~0.09~~	~~0.08~~	~~0.96~~	~~0.99~~	~~0.57~~
~~6dS-50~~					
~~a~~	~~0.40~~	~~0.06~~	~~0.15~~	~~1.27~~	~~0.16~~
~~b~~	~~0.35~~	~~0.14~~	~~0.39~~	~~0.98~~	~~0.24~~
~~c~~	~~0.35~~	~~0.34~~	~~0.96~~	~~0.98~~	~~0.24~~

~~Table 3. Concordance parameters for the four transects at depth 40-60cm. The table reports the Concordance, ρ_L, and the Pearson, ρ_P, correlation, as well as parameters α and β of the MRA line. The bias factor, C_b, is also shown.~~

~~Graph panel~~	**~~C_b 60cm~~**	**~~ρ_L 60cm~~**	**~~ρ_P 60cm~~**	**~~β 60cm~~**	**~~α 60cm~~**
~~1dS-100~~					
~~a~~	~~0.03~~	~~0.002~~	~~0.07~~	~~4.69~~	~~0.25~~
~~b~~	~~0.01~~	~~0.003~~	~~0.24~~	~~1.48~~	~~0.40~~
~~c~~	~~0.01~~	~~0.01~~	~~0.96~~	~~1.48~~	~~0.40~~
~~1dS-50~~					
~~a~~	~~0.08~~	~~-0.01~~	~~-0.12~~	~~4.81~~	~~0.05~~
~~b~~	~~0.04~~	~~-0.01~~	~~-0.17~~	~~2.14~~	~~0.22~~
~~c~~	~~0.04~~	~~0.04~~	~~0.96~~	~~2.14~~	~~0.22~~
~~6dS-100~~					
~~a~~	~~0.16~~	~~-0.01~~	~~-0.09~~	~~3.52~~	~~-0.60~~
~~b~~	~~0.09~~	~~-0.02~~	~~-0.25~~	~~1.43~~	~~0.22~~
~~c~~	~~0.09~~	~~0.08~~	~~0.96~~	~~1.43~~	~~0.22~~
~~6dS-50~~					
~~a~~	~~0.24~~	~~-0.07~~	~~-0.27~~	~~1.11~~	~~0.19~~
~~b~~	~~0.15~~	~~-0.03~~	~~-0.18~~	~~0.67~~	~~0.28~~
~~c~~	~~0.15~~	~~0.15~~	~~0.96~~	~~0.67~~	~~0.28~~